2011

Low Power Wake-up Signaling for Dense Sensor Networks

Ahmed M. Abuseta Ammar
West Virginia University

Low Power Wake-up Signaling for Dense Sensor Networks

by

Ahmed M. Abuseta Ammar

Thesis submitted to the
College of Engineering and Mineral Resources
at West Virginia University
in partial fulfillment of the requirements
for the degree of

Master of Science
in
Electrical Engineering

Matthew C. Valenti, Ph.D.
Natalia A. Schmid, Ph.D.
Daryl S. Reynolds, Ph.D., Chair

Lane Department of Computer Science and Electrical Engineering

Morgantown, West Virginia
2011

Keywords: Near field magnetic induction, wireless sensor networks, wake-up energy efficiency

Abstract

Low Power Wake-up Signaling for Dense Sensor Networks

by

Ahmed M. Abuseta Ammar

In wireless sensor networks, nodes are required to reduce their idle listening time in order to minimize energy consumption and increase their lifetime. The idle listening time is decreased by making the nodes remain in sleep mode and wake up only when they are required to sense or transmit information about an event. This strategy requires the source node to send a wake-up signal before it transmits data to the network. This wake-up signal requires energy and the objective of this work is to lower this signal's energy consumption.

In order to achieve this, this work uses Near Field Magnetic Induction Communication technology (NFMIC) that can communicate wirelessly over short distances using low power. Using this technology, the wake-up signal will be magnetic field lines rather than an RF signal. When a source node wants to wake up its neighbors, it generates magnetic field lines disseminating as bubbles. These lines resonate across the receiver coils of neighboring nodes, thus interrupting the sleeping nodes and waking them. This idea was implemented on a node using three different NFMIC systems. Each system had different combinations of TX and RX coils and communicated using different transmitted power. The most effecient setup was determined based on the wakeup energy efficiency. Finally, this work presents the effect of obstacles on NFMIC systems by testing them on one of our NFMIC systems. As a result of this test, the various obstacles were classified into three categories based on their attenuation effect.

Acknowledgements

I would like to express my gratitude to all those who participated and shared their ideas in this work to make it possible.

I would like to thank my committee chair and advisor, Dr. Daryl Reynolds, for his knowledge and assistance throughout my thesis. I sincerely want to thank him for giving me the opportunity to work with him and be one of his students. Besides him, I would like to thank Dr. David Graham for his knowledge and ideas, and his PhD student Brandon D. Rumberg for his hardware experience.

My sincere thanks go to Dr. Matthew C. Valenti and Dr. Natalia A. Schmid for being on my committee. In particular, I would like to thank Dr. Matthew C. Valenti for his guidance and advice, and I really appreciate his genuine concern towards students.

I dedicate this work to my father Mohammed Abuseta, and my mother Lazem Mohammed who I owe my success to after Allah. I am thankful and grateful to them for their patience, love, compassion, and support throughout my life. I also dedicate this work to the Libyan martyrs who have been killed in the revolution of February 17^{th} and the freedom fighters who are still struggling to get rid of the tyrant.

Finally, I would like to thank my friends Essa Tabar and Ali Omran for their moral support during my stay at WVU.

Contents

List of Figures

List of Tables

Notation

We use the following notation and symbols throughout this thesis.

TX	:	Transmitter
RX	:	Receiver
r_1	:	Radius of the transmitter coil
r_2	:	Radius of the receiver coil
M	:	Mutual Inductance
K	:	Inductive coupling
L_1	:	Inductance of the transmitter coil
L_2	:	Inductance of the receiver coil
C_1	:	Capacitance at the transmitter circuit
C_2	:	Capacitance at the receiver circuit
i_1	:	Current passes through transmitter circuit
i_2	:	Current passes through receiver circuit
i_{1rms}	:	RMS value of i_1
B	:	Magnitude of magnetic field
B_{pp}	:	The peak to peak value of the magnetic field
P	:	The point at which we want to know magnitude of magnetic field
d	:	Distance between wire and point P
l	:	The integration-path along the wire
dl	:	Small length of wire which carries current i_1
$\vec{d}$	:	Vector indicates to the direction of magnetic field towards P
μ_o	:	Permeability of the free space
x	:	Communication distance
N_1	:	Number of turns of the transmitter coil
N_2	:	Number of turns of the receiver coil
ϕ	:	Magnetic flux
V_{IND}	:	Induced voltage
A_1	:	Surface area of the transmitter coil
A_2	:	Surface area of the receiver coil
ω	:	Operating angular frequency
ω_o	:	Resonant angular frequency

$\Delta\omega$	:	difference between ω and ω_o
f_o	:	Resonant frequency
R_s	:	Internal resistance of the source
R_{L_1}	:	DC resistance of the transmitter coil
R_{L_2}	:	DC resistance of the receiver coil
R_L	:	Load resistance
R_{dc}	:	DC resistance of the transmitter or receiver circuit
R	:	Resistance added to the transmitter in order to calculate P_{Tx}
v_o	:	The peak to peak value of source voltage
v_s	:	Source voltage
V_L	:	Amplitude of received voltage signal
V_{L_1}	:	Voltage across transmitter coil
I_p	:	Peak value of current
Q_1	:	Quality factor of the transmitter cicuit
P_{TX}	:	Transmitted power
P_{RX}	:	Received power
X_{L_1}	:	Inductive reactance of the transmitter coil
X_{C_1}	:	Capacitive reactance of the capacitor at the transmitter circuit
τ	:	Width of a single pulse
n	:	Total number of pulses required to wake up the sensor at a certain distance
E_p	:	Energy consumed by one pulse
E	:	Energy consumed by n pulses

Chapter 1

Introduction

1.1 Introduction

Near Field Magnetic Induction Communication (NFMIC) is a short-range wireless technology that allows devices to communicate over short distances using low power [1]. The devices using this technology communicate through the coupling of magnetic fields rather than the propagation of electromagnetic waves as in far field communications [2, 3, 4]. In other words, the transmission energy in near field is contained within the localized magnetic fields and it resonates around the system, but does not radiate into free space the way it does in far field. This transmission energy attenuates or rolls off at a rate proportional to the sixth power of the communication distance ($1/d^6$). This makes Near Field Magnetic Induction Communication (NFMIC) systems feasible only over short distances compared to far field systems, where transmission energy attenuates at a rate ($1/d^2$).

In spite of the disadvantages of communicating over short distances, the way in which NFMIC systems communicate leads to some desirable features [5]. These features include lower power consumption, available bandwidth, and increased reliability. The availability of bandwidth is due to the fact that the devices do not need to compete against anything in the crowded RF spectrum, and the fact that each user is limited within his or her own small bubble (range of magnetic field) so that a frequency reuse technique can be exploited. As for the reliability, because of the rapid decaying of magnetic field over distance, the devices using NFMIC do not need to contend with fading due to multipath as in far field communication

devices. This property makes NFMIC devices more reliable than far field communication devices.

These features make NFMIC technology suitable for various applications. In particular, it is commonly used in the applications that require secure access. This is opposite to RFID technology applications in which security is not important. In RFID technology, communication is done through the use of radio waves and it is limited to transfer data between a reader and an electronic tag only when the reader asks for the data, i.e. the tag cannot communicate with the reader unless the reader wants to. In NFMIC technology, communication is done through the coupling of magnetic fields and both the terminals can communicate with each other whenever they want using low power. These advantages were the motivation of using NFMIC technology in the application of this work. Also, the motivation of using it in some other applications like biomedical monitoring [6], secure payment with NFC mobile phones [7], and NFC-enabled mobile phones for public health [8].

Of course, in these applications communication is achieved by having a transmitter and receiver, where the transmitter uses a coil to generate a magnetic field extending to a certain range at the time the receiver is placed within that range. The magnetic field resonates around the coil in the receiver, inducing a voltage having the same characteristics of the transmitted signal with opposite polarity. The magnitude of this voltage depends on the strength of the magnetic field which in turn depends on the physical specification of the transmitter (TX) coil. Also, the magnitude depends on the physical specification of the receiver (RX) coil and the communication distance between the transmitter and receiver. Maximizing this distance at lower transmitted power was the primary objective in this work before implementing the wake-up application using NFMIC technology.

In wireless sensor networks, the energy performance of nodes could be improved by reducing the duration of idle listening time. This time occurs when the radio in a node is left turned on when there is no data to be transmitted or received. Reducing this time can be implemented using methods such as periodically listening on the radio channel, as performed by the B-MAC algorithm [9]. In this algorithm, the power consumption of nodes was reduced and their lifetime was extended. However, these two factors were further improved using SpeckMAC-B and SpeckMAC-D algorithms [10]. In these algorithms, the savings in energy

were achieved by using wakeup signals of lower power as compared to B-MAC. Wakeup signal is the signal needed to be sent from the transmitter in order to inform its neighbors of impending data transfer. In B-MAC, the wakeup signal is an extended preamble while in the two SpeckMAC algorithms, it is wakeup frames and retransmission of the data packet, respectively. In our case, these wakeup signals could be the same but in a form of magnetic field lines rather than RF signals. This can be implemented using NFMIC technology that communicates using magnetic fields. Since magnetic fields consume low energy, we believe that this will help in saving more energy spent in wakeup signals and extend the lifetime of nodes in dense sensor networks, for example, extending the lifetime of nodes in embedded sensor network in the concrete which monitors the health of concrete in bridges and buildings.

In order to implement this idea, we first optimized our NFMIC system based on power efficiency and communication range. We then applied our wake-up application on it using $TelosB$ mote. The approach of this application is that the interrupt pin of $TelosB$ mote is connected to the output of a receiver circuit of an NFMIC system through an interface circuit. The purpose of this circuit is to match the impedance between the receiver circuit and the mote, to amplify the received signal, and to make the decision whether to wake up the mote or not. When a transmitter circuit sends a wakeup signal as magnetic field lines, these lines resonate across the receiver circuit generating a voltage signal. This signal will be passed to the mote as a DC signal voltage using the interface circuit to wake it up. Following this approach, in chapter 6, this work will show that the amount of the energy consumed by a wakeup signal using an NFMIC system is several μ joules when the communication distance is 90 cm.

1.2 Thesis Outline

In order to implement this work, it was necessary for us to understand the basic concepts of NFMIC technology. Chapter 2 describes the mechanism of this technology including the basic forms of the transmitter and receiver circuits. It also expresses theoretically the equations for calculating some variables like magnetic field strength, transmitted power, received power, and bandwidth. In addition, it shows the parameters that the strength of

magnetic field primarily depends on, and the way it can be increased in order to get higher communication distance at lower transmitted power.

Chapter 3 explains the experimental methodology of NFMIC system described in chapter 2. In details, it explains the way this system is practically connected, and how some variables are measured like transmitted power, received power, resonant frequency, and communication distance. In the case of measuring the transmitted power, we could not measure the current directly in order to calculate it due to the limitation of our current meters. However, we measured it in an indirect way as it will be explained in the chapter.

Chapter 4 shows the results of the experiments which were performed on some NFMIC systems in order to expand the communication distance at lower transmitted power. It also shows how the experimental results match with theoretical results, and how these experimental results reinforce the interpretations that were made earlier about some facts and equations in chapter 2. From these experiments, we selected three systems based on power efficiency to be used in the following two chapters.

Chapter 5 examines the effect of obstacles on NFMIC systems. The obstacles which were tested includes a wall, cardboard, metal box, wooden box, and concrete. Chapter 6 contains the application of wake-up signal. In this application, the energy required to wake up the node was calculated with respect to the communication distance for three different systems. For the system with the best energy performance, the energy was recalculated at three different noise levels and the average value was determined. Finally, chapter 7 reviews the conclusion and includes some ideas for future research.

Chapter 2

Theoretical Analysis

Figure 2.1 shows the block diagram of a simple NFMIC system. The communication link of such a system is established based on the magnetic inductive coupling between transmitter and receiver coils whereby these two coils are parallel and aligned on a common central axis. This is to ensure the maximum magnetic field resonating across the receiver coil in order to receive the best signal. As shown in the figure, the transmitter and receiver coils have radii r_1 and r_2, respectively, and they are separated from each other by a distance d. Since the medium between the coils is free space, the inductive coupling can be estimated as $K = \frac{M}{L_1 L_2}$ where L_1 and L_2 are the inductances of TX and RX coils, respectively, and M is the mutual inductance between the two inductive circuits shown in Figure 2.2 and it is defined as the effect of producing of an electromotive force (EMF) in RX coil because of the change in current passing in TX coil [11].

Figure 2.2 illustrates the equivalent circuit model for an NFMIC system. Based on this equivalent circuit and the block diagram shown in Figure 2.1, we can derive a formula expressing the induced voltage across the receiver coil at any point placed along the axis of the transmitter coil as a function of distance. In addition, we can derive two other formulae. One expresses the power transfer from the transmitter to receiver while the other expresses the received power as a function of the separation distance. Of course, before deriving these formulae, we need to calculate the magnitude of the magnetic field produced by the TX coil. In the following sections, we will show how to calculate the magnitude of the magnetic field and derive the three formulae.

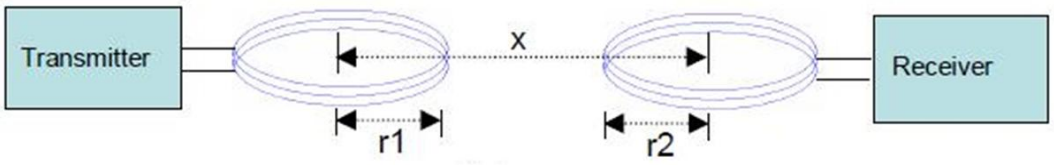

Figure 2.1: Inductively coupled NFMIC system [12].

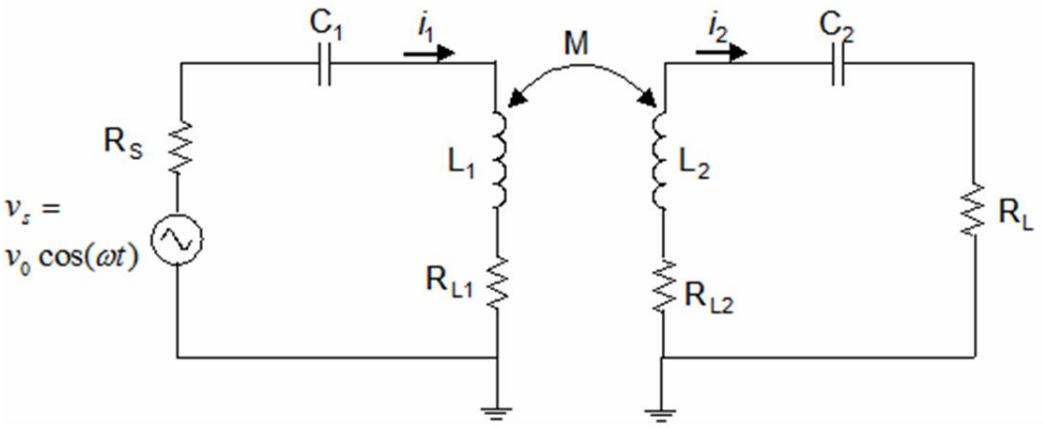

Figure 2.2: Equivalent circuit model for a NFMIC system [12].

2.1 Calculating the Magnetic Field Strength

According to Ampere's law [13], a simple way to generate a magnetic field is by passing a steady current through a wire. The strength of this magnetic field increases as the steady current increases. However in the case of using a coil instead of a wire, the strength of the magnetic field not only increases with increasing steady current but also with increasing the number of turns and radius size. This fact will be shown later after we derive the equation of magnetic field strength at distance x. The equation of the magnetic field strength in the case of wire can be found using Biot-Savart law [14].

Biot-Savart law is named after the two French professors Biot and Savart, who collaborated together and came up with this law. It was derived to calculate the magnetic field strength produced by a current passing through a wire. According to this law, if we consider the wire shown in Figure 2.3 carrying a current i_1, the magnetic field B generated by the

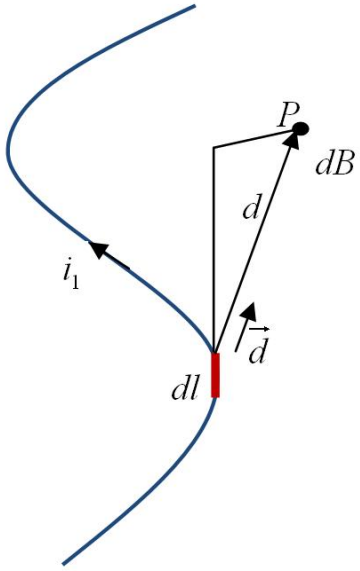

Figure 2.3: A wire caries a current i_1 generating a magnetic field B around it.

path at point P at distance d from the wire is given by

$$B = \frac{\mu_o}{4\pi} i_1 \int \frac{dl \cdot \vec{d}}{d^2} \qquad \text{Wb/m}^2, \tag{2.1}$$

where μ_o is the permeability of the free space, dl describes the infinitesimal length of the wire, and Wb/m^2 is Weber per meter square, unit of magnetic field.

Now, instead of wire, consider that we have a single loop coil with radius r_1 carrying a current i_1 as shown in Figure 2.4. Assume we want to find the strength of the magnetic field B at point P at distance d from the coil. Also, assume that point P is located along the central axis of the coil. In this case, all the terms in the loop are constant except the distance element dl, which when integrated in (2.1) just gives the circumference of the circle. The strength of magnetic field at distance d generated by the loop is then

$$B = \frac{\mu_o i_1 2\pi r_1}{4\pi d^2} \cos\theta. \tag{2.2}$$

From Figure 2.4, $\cos\theta = \frac{r_1}{d}$ and $d = \sqrt{{r_1}^2 + x^2}$, where, x stands for the distance from the center of the coil to the point P. Substituting the parameters in (2.2), the strength of the magnetic field equation can be written as

$$B = \frac{\mu_o i_1 {r_1}^2}{2\left({r_1}^2 + x^2\right)^{3/2}}. \tag{2.3}$$

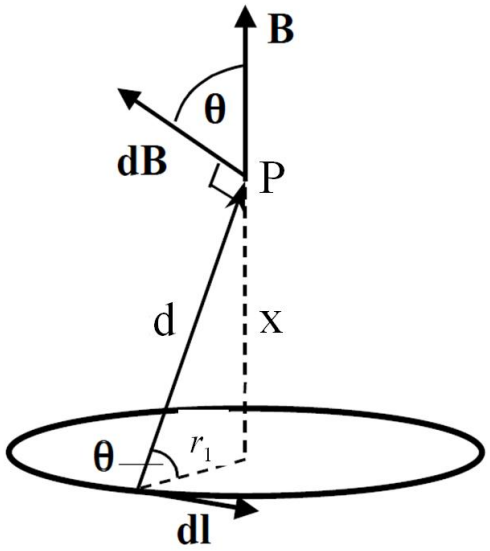

Figure 2.4: A single loop coil caries a current i_1 generating a magnetic field B around it.

If we replace the single coil with a coil having N_1 turns, we can rewrite (2.3) as

$$B = \frac{\mu_o i_1 {r_1}^2 N_1}{2({r_1}^2 + x^2)^{3/2}} \qquad \text{Wb/m}^2. \tag{2.4}$$

Equation (2.4) proves what we stated earlier, i.e that the magnitude of a magnetic field in the case of coil is proportional not only to current flowing through but also to number of turns and size of radius. This is because the magnetic field in the case of a coil is a result of adding all magnetic fields produced by each loop or turn. Furthermore, it turns out that the magnetic field strength of a coil with N_1 turns is equal to N_1 times the magnetic field strength of a coil with single loop. Finally, this holds true to the case when the current i_1 is time-variant. However, this results in a time-variant magnetic field instead.

2.2 Calculating the Induced Voltage Across the Receiver Coil

The induced voltage across the receiver coil is produced due to a phenomenon called electromagnetic induction [15]. This phenomenon was first noticed and investigated by Faraday. It states that the induced voltage is proportional to the rate of change of the

magnetic field across the closed surface, which in our case is a loop. As we have seen in Section 2.1, a time-variant magnetic field can be generated by passing a time-variant current through a coil and the magnitude of such a magnetic field can be calculated from (2.4).

A simple equivalent model of an NFMIC system is shown in Figure 2.1. The model shows the transmitter and receiver circuits. When the RX coil is placed within the near field range of the TX coil, the time-varying magnetic field, which is produced by TX coil due to a time varying current, induces a voltage called electromotive force (EMF) in the RX coil. The induced voltage causes a flow of current i_2 in the coil. This is called Faraday's Law [16]. The induced voltage in the RX coil is equal to the rate of change of the magnetic flux ϕ over time t. This is expressed as

$$V_{IND} = -N_2 \frac{d\phi}{dt}, \tag{2.5}$$

where V_{IND} is the magnitude of induced voltage in RX coil, N_2 is number of turns in the RX coil, and ϕ is magnetic flux through each turn in Weber (Wb). We can find the magnetic flux density ϕ that represents the total magnetic field that is passing through the entire surface of the coil as

$$\phi = \int \vec{B} \cdot d\vec{A}_2 \qquad \text{Wb}, \tag{2.6}$$

where B is the magnetic field strength given by (2.4), A_2 is the surface area of the RX coil and $\cdot$ represents the inner product between the two vectors $\vec{B}$ and $d\vec{A}_2$. The value of ϕ is dependent on the cosine angle between the two vectors. If we assume the angle between these two vectors is θ, the magnetic flux density equation can be modified as

$$\phi = A_2 B \cos\theta. \tag{2.7}$$

Following from (2.5) and (2.7), the induced voltage is expressed in terms of magnetic field strength, number of turns, and surface area of the RX coil as

$$V_{IND} = -N_2 A_2 \cos\theta \frac{dB}{dt}. \tag{2.8}$$

The minus sign in the equation shows that the induced voltage across RX coil opposes the voltage signal generated by the source in TX circuit. It means the change in the magnetic

field in the RX coil produced due to the induced current i_2 opposes the change in magnetic field generated by the TX coil. This is known as Lenz's Law [17], which states that the induced current generated by a magnetic field produces an induced magnetic field that is opposite in direction to the magnetic field generating the induced current.

If we assume that current i_1 varies sinusoidally with time, the generated magnetic field will also vary sinusoidally with time. This magnetic field strength can be expressed as

$$B = \frac{1}{2} B_{p-p} \cos \omega t, \tag{2.9}$$

where B_{p-p} is the peak to peak value of the magnetic field strength, and ω is the angular frequency of alternating current i_1. If we combine (2.8) and (2.9), the equation of induced voltage across the RX coil becomes

$$V_{IND} = \frac{1}{2} \omega N_2 A_2 B_{p-p} \cos \theta \sin \omega t. \tag{2.10}$$

Let us consider that V_{p-p} is the peak to peak value of the induced voltage and it is measured for $\theta = 0$. The equation for calculating this voltage can be given as

$$V_{p-p} = \omega N_2 A_2 B_{p-p} \qquad \text{V}. \tag{2.11}$$

Equation (2.11) shows that the induced voltage V_{p-p} will rise substantially if the RX coil's inductance L_2 is tuned to the frequency of the transmitter signal. We can tune the coil to this frequency by connecting a capacitor in a series with it as shown in Figure 2.2. The equation also indicates that the induced voltage will increase proportional to the generated magnetic field B_{p-p}. We have proved earlier that the magnitude of magnetic field is proportional to the radius and number of turns of the TX coil. In addition to this, the equation shows that the induced voltage is proportional to the surface area and number of turns of the RX coil. In conclusion, one can say that increasing the radius size and number of turns of TX and RX coils induces a higher voltage. Higher induced voltage means higher communication range or maximum distance at which the received signal is equal to the minimum required received signal power.

2.3 Computing Transmitted Power

The transmitted power of the system is computed from the transmitter circuit shown in Figure 2.2. R_{L_1} is the DC resistance of the transmitter coil; C_1 is the capacitor which is used to resonate the coil at the operating frequency; and R_s is the internal resistance of the source. From the circuit, we can find the current i_1 at angular frequency near to the angular resonant frequency ω_o as

$$i_1(\omega) = \frac{v_o}{(R_{L_1} + R_s)\left(1 + j\frac{2Q_1\Delta\omega}{\omega_o}\right)}, \tag{2.12}$$

where, Q_1 is quality factor of the TX circuit ($Q_1{=}\frac{\omega_o L_1}{R_{L_1}+R_s}$), $\Delta\omega$ is the difference between operating angular frequency and resonant angular frequency ($\Delta\omega{=}\omega-\omega_o$), and ω_o is angular resonant frequency ($\omega_o{=}\frac{1}{\sqrt{L_1C_1}}$).

If the transmitter is resonated at the angular resonant frequency, it means that ($\omega = \omega_o$), and the inductive and capacitive reactances are equal in magnitude but cancel out each other because they are 180 degrees apart in phase. This enables the maximum current to flow through the coil generating maximum magnetic field intensity. At this frequency the maximum current is given as

$$i_1(\omega_o) = \frac{v_o}{(R_{L_1} + R_s)} \qquad \text{A.} \tag{2.13}$$

The source voltage shown in Figure 2.2 generates a sinusoidal voltage signal. As a result, i_1 will be a sinusoidal current signal. To calculate the power generated by this current, we need to convert this current from peak to peak value to RMS value. If $i_{1(rms)}$ represents the RMS value to the current i_1, the maximum transmitted power generated by the TX coil can be calculated using

$$P_{TX} = {i_1}^2{}_{(rms)} R_{L_1} \qquad \text{W.} \tag{2.14}$$

2.4 Computing Received Power

The received power of the system shown in Figure 2.2 can be calculated from the RX circuit. When the varying magnetic field resonates across the RX coil, it generates an

alternating voltage in it. This voltage produces a current i_2 and that flows through the RX circuit generating a voltage drop signal across the load R_L . This signal is considered to be the received signal. It has the same characteristics of TX signal but with lower amplitude due to the attenuation between TX and RX. By applying voltage divider in the RX circuit, we can find the voltage amplitude of the received signal V_L across the load at the resonant frequency ω_o=$\frac{1}{\sqrt{L_2C_2}}$ as

$$V_L = V_{IND}\frac{R_L}{R_L + R_{L_2}} \qquad \text{V.} \tag{2.15}$$

Now, the available power from the TX that is delivered to the load is given as follows

$$P_{RX} = \frac{{V_L}^2}{R_L}. \tag{2.16}$$

Following from (2.15) and (2.16) the received signal is expressed in terms of the induced voltage as

$$P_{RX} = \frac{V_{IND}^2 R_L}{\left(R_L + R_{L_2}\right)^2}. \tag{2.17}$$

From (2.4) and (2.11), (2.17) can be rewritten as

$$P_{RX} = \frac{\left(\mu_o \omega N_2 A_2 N_1 {r_1}^2 i_1\right)^2}{4\left({r_1}^2 + x^2\right)^3}\frac{R_L}{\left(R_L + R_{L_2}\right)^2}. \tag{2.18}$$

For $x \gg r_1$ and $R_L \gg R_{L_2}$

$$P_{RX} = \frac{\left(\mu_o \omega N_2 A_2 N_1 {r_1}^2 i_1\right)^2}{4R_L}\frac{1}{(x^6)} \qquad \text{W.} \tag{2.19}$$

Equation (2.19) indicates that the transmitted power produced by TX circuit decays at a rate proportional to $1/x^6$. This near field decaying behavior of the transmitted power is different from far field, in which the transmitted power decays at a rate proportional to $1/x^2$ according to $Friis$ transmission equation [18]. This slow attenuation of far field over distance allows communication systems to communicate effectively over long ranges. This is opposite to near field in which systems are limited in communication range due to the rapid decaying of their transmitted power. In terms of security and frequency reuse, this property of near field is considered an advantage since the coverage area is small and each user is limited with his or her magnetic field range.

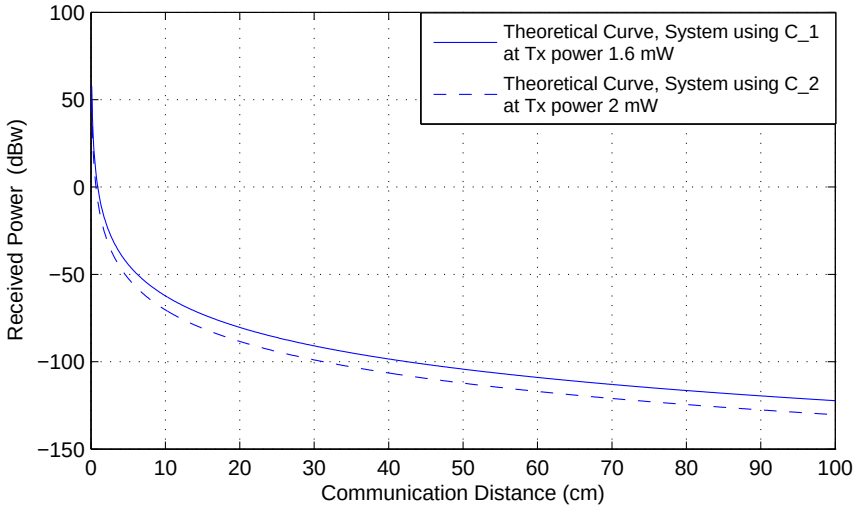

Figure 2.5: Plots of the theoretical received power versus communication distance for the system using C_1 and the system using C_2 as antennas.

Coil	Symbol	Resistance	Wire Gauge (AWG [19])	#of Turns	Diameter
Coil 1	C_1	12Ω	30	650	2.5 cm
Coil 2	C_2	5.2Ω	30	400	1.9 cm

Table 2.1: The parameters of the two coils that were designed and fabricated in our Lab.

Figure 2.5 shows the simulation results of (2.19) for two NFMIC systems using two models of coils C_1 and C_2 that were designed and manually wound in our Lab. In the first system, the coil C_1 was considered to be used as TX and RX antennas and operated at frequency 263 KHz and transmitted power 1.6 mW. While in the second system, the coil C_2 was considered to be used rather than C_1 and operated at frequency 590 and transmitted power 2 mW instead. Using this information, transmitted power and operating frequency, and the physical specifications of the two coils shown in Table 2.1, the simulation results of (2.19) for the two NFMIC systems were as shown in Figure 2.5. The figure illustrates two facts mentioned earlier. First, the transmitted signal decays rapidly over distance. The figure illustrates two facts mentioned earlier. First, the transmitted signal decays rapidly over distance. Second, communication range increases on using coils with a higher radius and number of turns. From the figure, the first fact can be seen clearly by comparing the values of received signal power of the system using C_1 as TX and RX antennas at the distances 1 cm and 20 cm. At these distances, the received power is approximately -2.5 dBw and -80 dBw, respectively. This means that the signal is attenuated by 77.5 dB over a short range 19 cm, which reflects the rapid decaying of NFMIC systems. The other fact can be noticed by comparing the maximum distance between the system using C_1 and the system using C_2 as antennas when the received power is equal to the minimum required received signal power. If we assume that the minimum required received signal power is -122 dBw, the maximum communication range of the system using C_1 is about 100 cm at transmitted power 1.6 mW. As for the system using C_2, the maximum communication range is about 80 cm although its transmitted power is 2 mW higher than the transmitted power of the system using C_1. This increase in the communication range at lower transmitted power is due to the higher radius and number of turns C_1 has compared to C_2. This result reinforces the interpretation provided earlier about (2.11) that increasing the radius size and number of turns of TX and RX coils induces a higher voltage. A higher induced voltage results in a higher communication distance. Finally, note that the transmitted power was calculated using (2.14) when the source voltage was a sinusoidal signal. In the two systems, system

using C_1 and system using C_2, the sinusoidal signal had a frequency 263 KHz and 590 KHz, respectively.

2.5 Bandwidth

In band pass filters, bandwidth can be defined as a measure of the width of the range of positive frequencies passed by the filter without significant attenuation. That means only signals with frequencies within this range will be passed, while frequencies outside the range will be rejected or attenuated. This type of filter can be created by combining a low pass filter with a high pass filter. Its bandwidth will be the difference between the upper and lower cutoff frequencies. Upper and lower cutoff frequencies are the frequencies at which the magnitude of the voltage gain or current gain drops by a factor of $\sqrt{2}$. In terms of quality factor and resonant frequency, bandwidth of such a filter can be considered as the ratio between the resonant frequency and the quality factor [20].

The transmitter, shown in Figure 2.2, is actually representing a band pass filter with output measured across the TX coil. To compute the bandwidth of this filter [21, 12], we need to find its quality factor, which can be found from the equation expressing the voltage gain of the filter. Since the filter (which is a series combination of R_{dc}, L_1, and C_1) forms a voltage divider, the voltage drop in the coil is given by

$$V_{L_1} = \frac{jX_{L_1}v_s}{R_{dc} + jX_{L_1} - jX_{C_1}} \qquad \text{V}, \tag{2.20}$$

which is equivalent to

$$V_{L_1} = \frac{jX_{L_1}v_s}{R_{dc}\left(1 + j\frac{X_{L_1} - X_{C_1}}{R_{dc}}\right)}. \tag{2.21}$$

Since the voltage gain is the ratio between the input and output voltages, it can be expressed as

$$\frac{V_{L_1}}{v_s} = \frac{jX_{L_1}}{R_{dc}\left(1 + j\frac{X_{L_1} - X_{C_1}}{R_{dc}}\right)}. \tag{2.22}$$

Now, the magnitude of the voltage gain is

$$\left|\frac{V_{L_1}}{v_s}\right| = \frac{X_{L_1}}{R_{dc}\sqrt{1+\left(\frac{X_{L_1}-X_{C_1}}{R_{dc}}\right)^2}}. \tag{2.23}$$

From (2.23), the quality factor of the transmitter circuit is equal to the magnitude of the voltage gain when ($\omega = \omega_o$), at which the reactance components cancel out each other such that $X_{L_1} = X_{C_1}$. This is equal to the ratio between the inductive reactance X_{L_1} and the DC resistance R_{dc}. R_{dc} represents the summation of the internal resistance of the function generator R_s and the DC resistance of the coil R_{L1}. The quality factor can be expressed as

$$Q_1 = \frac{X_{L_1}}{R_{dc}} = \frac{2\pi f_o L_1}{R_{dc}}. \tag{2.24}$$

In terms of the quality factor, the bandwidth of the transmitter can be given by

$$BW = \frac{f_o}{Q_1} = \frac{R_{dc}}{2\pi L_1} \qquad \text{Hz.} \tag{2.25}$$

We can see then that the relationship between resistor R_{dc} and inductor L_1 determines the bandwidth of the transmitter. The bandwidth is proportional to R_{dc} and inversely proportional to L_1.

Chapter 3

Experimental Methodology

This chapter is intended to describe the experimental methods for verifying the analytical expressions that were described in the previous chapter. During the chapter, we will show the practical layout of NFMIC systems which were being used to do all the experiments throughout this work. Also, we will experimentally explain the way to compute the TX and RX power of an NFMIC system, and illustrate the way to determine its resonant frequency. Finally, we will practically show how to calculate the maximum communication range of an NFMIC system.

3.1 NFMIC System Layout

A practical NFMIC system equivalent to the model shown in Figure 2.2 is illustrated in Figure 3.1. As depicted on the left side of the diagram, the transmitter has a series combination of a capacitor and TX coil. The combination is attached to a function generator which has an internal resistance 50 Ω, and it can provide sinusoidal, square, and triangle signals with frequencies up to 20 MHz and amplitude up to 20 V_{p-p} . On the right side of the diagram, the receiver has a series combination of a capacitor and RX coil. But this time, the combination is attached to an oscilloscope rather than a function generator to read the received signal. The oscilloscope can read signals with a wide range of amplitude and frequency up to 13.5 MHz . It has 1 MΩ as input resistance, and 13 pF as input capacitance. The capacitance is one of the factors that affects the resonant frequency of the system.

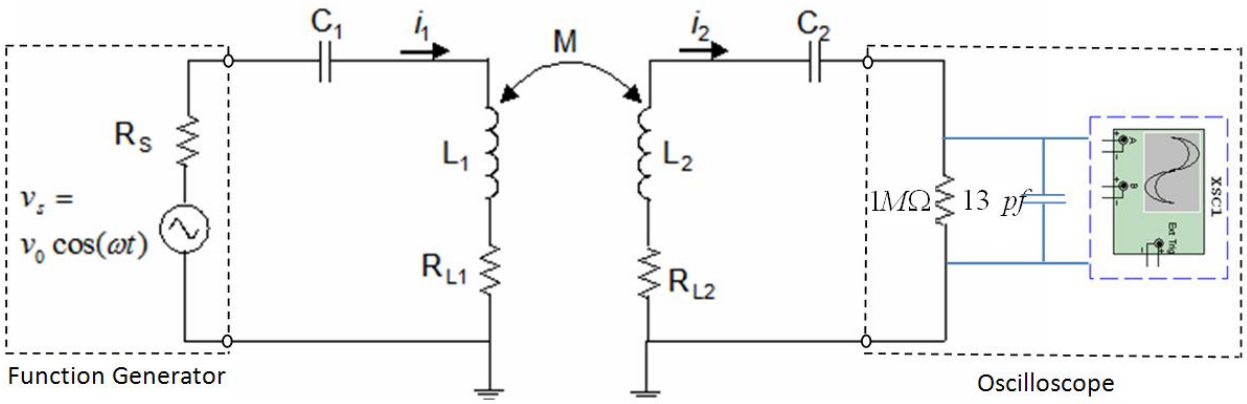

Figure 3.1: A practical NFMIC system equivalent to the model shown in Figure 2.2.

3.2 Measuring TX and RX Power

The way we measure the TX and RX power of NFMIC system is by using (2.15) and (2.17) and measuring the parameters practically instead of calculating them theoretically. In the case of computing the received power, we measure the magnitude of the received voltage signal V_L using the oscilloscope across the load R_L , and we then substitute these parameters in (2.17) to get the practical value of the received power. As for the transmitted power, we measure the actual magnitude of $i_{1(rms)}$ and then use (2.15) to calculate it since the value of R_{L_1} is already known. The way we measure $i_{1(rms)}$ is by

1. Connecting a resistor R in series with the coil as shown in Figure 3.2.
2. Measuring the voltage drop across it using the oscilloscope.
3. Calculating the magnitude of $i_{1(rms)}$ from these two values using Ohm's law.

This way of measuring $i_{1(rms)}$ was used instead of measuring it directly because the devices we have in the Lab cannot measure currents with frequencies higher than 40KHz.

As for the value of the resistor R_L, it depends on the value of R_{L_1}, the DC resistance of the transmitter coil. It is usually chosen to be very small relative to the value of R_{L_1} so that the magnitude of the current measured when the resistor R_L exists is close to the actual value when the resistor does not exist. This reduces the error in measuring the actual power and makes the measured power close to the actual power.

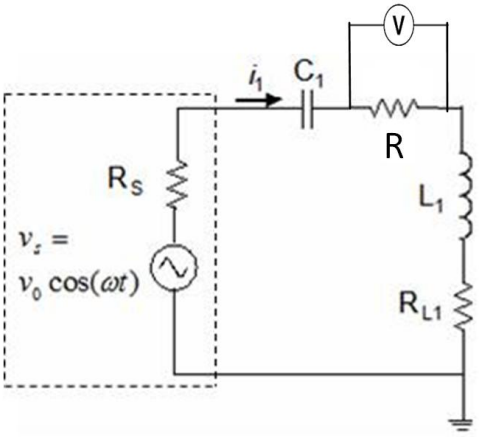

Figure 3.2: TX circuit showing how the resistor R is added to calculate the magnitude of $i_{1(rms)}$.

3.3 Resonant Frequency

Experimentally, we set the resonant frequency of our NFMIC systems to the frequency at which the received signal is maximized and not to the frequency that is calculated theoretically from $\omega_o = \frac{1}{\sqrt{LC}}$ [22]. This is because the size of the capacitor C is changed due to two reasons. The first reason is that the breadboard itself which is used to assemble the components of TX and RX circuits has a capacitance. This capacitance varies the size of C and makes the resonant frequency different from the frequency calculated theoretically. The other reason is caused by the input capacitance of the oscilloscope that is attached to the receiver circuit as shown in Figure 3.1. This capacitance also affects the capacitance size C and changes the resonant frequency.

In order to determine the frequency at which the received signal is maximized, we position both of the TX and RX circuits from the coils' side very close to each other with near zero separation distance. We then apply a sinusoidal voltage signal on the TX circuit from the function generator and read it using the oscilloscope at the receiver. At the transmitter, we vary the frequency of the signal gradually starting from the minimum value. At the same time, we observe the amplitude of the signal on the oscilloscope. While changing the frequency, the amplitude of the signal increases until approaching f_o. At f_o the amplitude peaks, and then decreases with increasing frequency. This frequency is considered to be the

resonant frequency of NFMIC system.

3.4 Communication Range

The maximum communication distance of a NFMIC system is determined by the size of the magnetic bubble, which is defined either in terms of the sensitivity of the receiver or in terms of the signal-to-noise ratio of the system. In terms of the receiver sensitivity, which is the minimum power in watts that can be sensed by the receiver, consider x is the distance at which the received signal power is equal to the sensitivity of the receiver. The radius of the magnetic bubble is defined as the distance x where the received power is equal to the sensitivity of the receiver. This radius can be even larger if the receiver is highly sensitive. As for the signal-to-noise ratio of the system, the radius of the magnetic bubble can be defined as the distance at which the received signal is just equal to the noise power. Based on the definition, this distance is considered to be the communication range of the system since beyond it the receiver only receives noise. In this work, the communication distance of an NFMIC system is defined as the distance at which the received power is equal to the minimum required received signal power. The minimum required received signal power is assumed to be equal to the noise power in the environment.

Chapter 4

Maximizing Communication Distance

This chapter shows the results for some experiments which were performed to achieve the goal of maximizing the communication distance at a lower transmitted power. Through the chapter, we will experimentally show how the parameters shown in (2.19) are varied to achieve our goal. In particular, we will study the effect of number of turns, diameter size, shape of transmitted signal and operating frequency on communication distance and transmitted power. We will show the transmitted power versus communication distance graphs for some different NFMIC systems. From the graphs, we will determine the system that has a better power efficiency versus communication distance characteristics. At the end, we will show that using coils with a higher number of turns at the transmitter increases the communication range but it reduces the bandwidth of the system.

4.1 Number of Turns and Diameter Size

In order to increase the communication range of a NFMIC system, we need to either extend the size of the magnetic bubble generated by the TX coil, or increase the sensitivity of the RX coil. Of course, increasing both of them at once will effectively contribute in maximizing the communication range. The way to extend the size of the magnetic bubble is by increasing the strength of the magnetic field resonating across the RX coil. As it has been proven in Section 2.1 and from (2.4), the strength of the magnetic field increases with increasing number of turns and radius size of the TX coil. As for the sensitivity of the RX

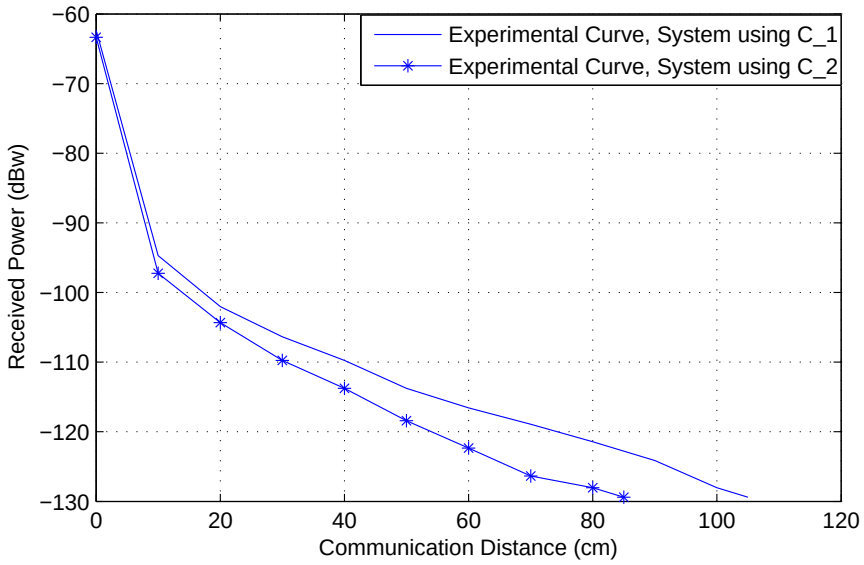

Figure 4.1: Plot of the experimental received power versus communication distance for the system using C_1 and the system using C_1 as antennas.

coil, it can also be increased by increasing the number of turns and radius size of the RX coil. This is because the strength of the magnetic field across the RX coil is equal to the summation of all magnetic fields across each loop or turn. Equation (2.11) shows that the induced voltage in RX coil is a function of number of turns N_2 and radius size r_2 . From the equation, we can also infer that the induced voltage in a coil with N turns is N times the induced voltage in a coil with one turn, regardless of the radius size of both the coils.

Theoretically, it has been shown clearly how the communication range of NFMIC systems depends on the physical specifications of the TX and RX coils. From (2.19) and Figure 2.5, the communication range for such systems can be increased by increasing the coils' radius size and number of turns. In order to prove this claim experimentally, we performed two experiments on two systems. In the first experiment, the system has C_1 with specifications shown in Table 2.1 as TX and RX antenna coils and operates at frequency 263 KHz. In the second experiment, the system operates at frequency 590 KHz and has C_2 as TX and RX antenna coils. Table 2.1 shows that this coil, C_2, has a lower number of turns and smaller radius size than C_1. Finally, in both the experiments, the system was connected as shown in Figure 3.1 and the source voltage was a sinusoidal voltage signal with frequency 263 KHz

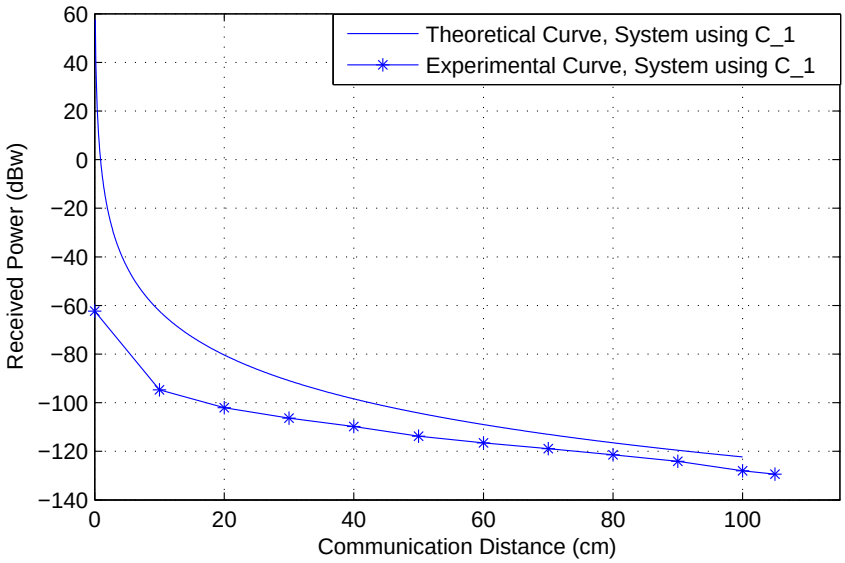

Figure 4.2: Plot of the experimental and theoretical received power versus communication distance for the system using C_1 as antennas.

and 590 KHz, respectively.

Figure 4.1 shows the results of the two experiments. Figures 4.2 and 4.3 show how the experimental results measured from the two experiments match the theoretical results. From Figure 4.1, we can notice that in the system using C_1, the received power of the signal is equal to the minimum required received signal power at a distance of approximately 105 cm. The minimum required received signal power in the place where the two experiments were performed was measured to about -129 dBw. From the figure we can also notice that in the system using C_2, the received power is equal to the minimum required received signal power at a distance of about 85 cm. This indicates that the system using C_1 has a higher communication range than the system using C_2, although the transmitted power in the first system was 1.6 mW, lower than 2 mw, the transmitted power in the second system. This higher communication distance at lower transmitted power in the first system is due to the higher number of turns and the larger radius size of the coils. This emphasizes the interpretation we made earlier about (2.11) that the communication distance of an NFMIC system is proportional to the number of turns and radius size of TX and RX antenna coils. Figures 4.2 and 4.3 indicate how far the experimental results differ from the theoretical

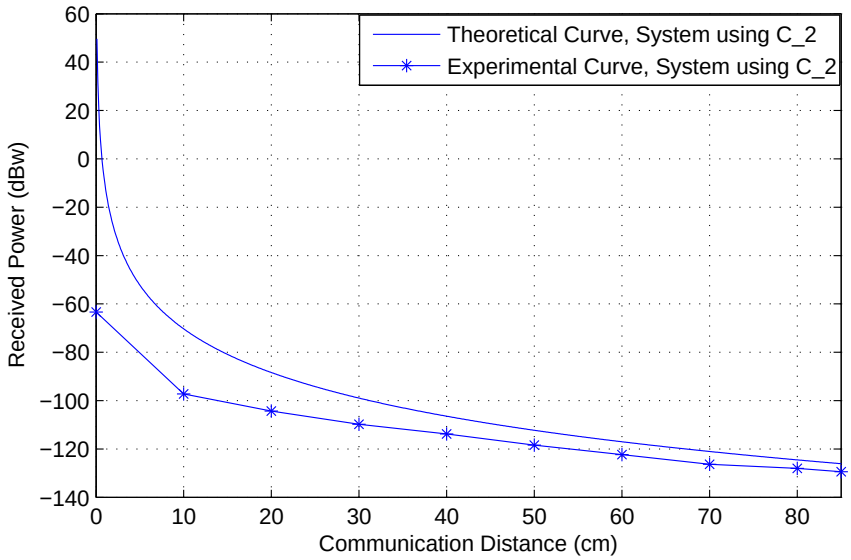

Figure 4.3: Plot of the experimental and theoretical received power versus communication distance for the system using C_2 as antennas.

results, and show that the gap between the two curves gets smaller as the distance increases.

The coils, C_1 and C_2, used in the two experiments were only designed to measure the validity of (2.19) and to get an idea about how near field magnetic induction communication systems work in practical life. They are not practical to be used as antennas due to the following reasons:

1. There is a loss in the magnetic field produced by these coils due to the gap left between the turns while winding them. As a result of this, the communication range will be affected and becomes lower.

2. The arbitrary winding by hand and the large diameter size of the wire used cause the coils to have a small number of turns in a large diameter size. The same diameter size can result in a higher number of turns if a wire with a higher gauge is used and wound in a neater way. As we learned earlier, a higher number of turns means a higher magnetic field strength and a higher magnetic field strength means a larger communication range.

3. The coils consume more power relative to the short distance they communicate over. This high consumption of power is because of the high current drained from the source due to the small DC resistance of the coils.

These disadvantages make the goal of maximizing the communication distance at low transmitted power not possible with these two coils. This problem led us to look for other coils wound in a neater way using a higher wire gauge. We started looking for a vendor who could help us design such coils since we do not have the facility or the machines to wind the coils ourselves as required. Table 4.1 shows the parameters for some of the T-Coils (telecoils) ordered from GlobalCoils Company. These coils were designated for hearing aid purposes and they were well made to have a high sensitivity to magnetic fields. After testing all possible combinations of these coils as TX and RX antennas, Table 4.2 shows the NFMIC systems with the best combinations in terms of communication distance and transmitted power. These systems were used to do the rest of the experiments in this work. They were connected the way shown in Figure 3.1 each with its operating frequency as shown in Table 4.2.

Coil Type	symbol	Resistance	Gauge	#of Turns	Diameter	Inductance
T-Coil#1	TC_1	1,250 Ω	36	$\succ$ 3500	2.1 mm	96 mH
T-Coil#2	TC_2	2,120 Ω	36	-	-	-
T-Coil#3	TC_3	1,900 Ω	36	-	2.16 mm	630 mH
T-Coil#4	TC_4	3,700 Ω	36	-	2.29 mm	900 mH
T-Coil#5	TC_5	1,4000 Ω	36	-	-	-

Table 4.1: The parameters of some ordered T-Coils

Coil Type	TX Coil	RX Coil	Resonant Frequency
System#1	TC_1	TC_1	60 Khz
System#2	TC_3	TC_1	60 Khz
System#3	TC_4	TC_1	60 Khz
System#4	TC_4	TC_2	60 Khz
System#5	TC_5	TC_1	100 Khz
System#6	TC_5	TC_2	60 Khz

Table 4.2: NFMIC systems with different combination of TX and RX T-Coils

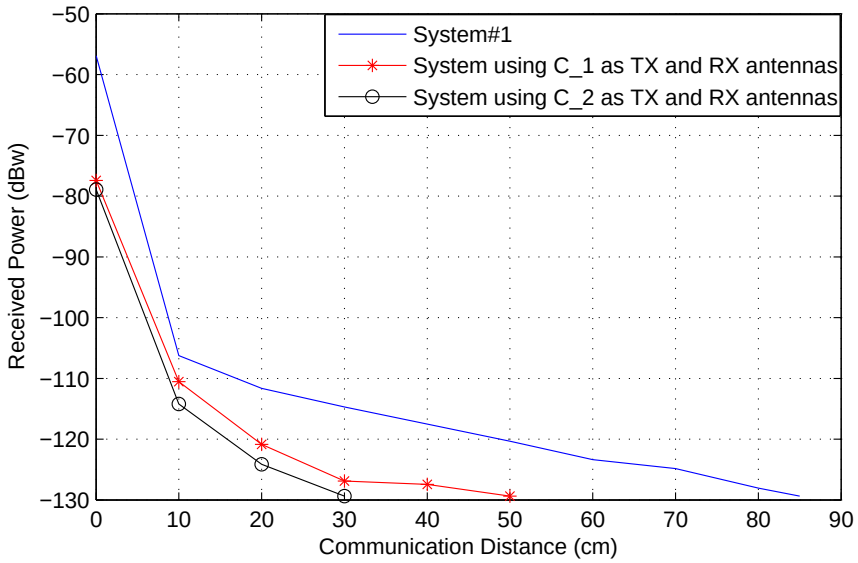

Figure 4.4: Plot of the received power versus communication distance for System#1 and the two systems that use C_1 and C_2 as antennas at the same transmitted power

Figure 4.4 illustrates the curves of the received power versus distance for System#1 that uses TC_1 as TX and RX antennas, and the two systems that use C_1 and C_2 as antennas, respectively. The curves were plotted at the same transmitted power of approximately 369.7 μW, which was calculated as described in section 2.3. In the three systems, this power was set to this value by adjusting the amplitude of the source voltage using (2.14), where the source voltage was a sinusoidal signal. The results show that System#1, using TC_1, can communicate up to 90 cm, while the systems using C_1 and C_2 can communicate up to 50 cm and 30 cm, respectively. This higher range of communication achieved by System#1 over the other two systems is due to the higher sensitivity and higher number of turns of TC_1. According to the manufacturing company, the coil has more than 3500 turns, which is more than five times the number of turns in each of C_1 and C_2.

TC_1 is the coil which has the smallest number of turns and lowest radius size among the five T-Coils shown in Table 4.1. This means that its generated magnetic field is lower than the generated magnetic field of the other T-Coils. We will show later in section 4.4 how we can take advantage of using these coils to maximize the communication distance at a transmitted power lower than 369.7 μW.

4.2 Shape of the Transmitted Signal

The transmitted power of an NFMIC system is the power consumed by the TX antenna coil and it is calculated as described in section 2.3. This power is a part of the total power consumed from the source. At the resonant frequency, the total power consumed from the source is equal to the transmitted power plus the power dissipated by the internal resistance of the source. If the internal resistance of the source is very small compared to the resistance of the TX coil so its consumed power could be neglected, these two kinds of power (the total consumed power and the transmitted power) may or may not be the same depending on the shape of the transmitted signal and the bandwidth. For example, if the bandwidth of an NFMIC system is narrow and the transmitted signal is a square wave [23], the transmitted power of the system will not be the same of the total power consumed from the source. This is because the only harmonic will pass through the system is the fundamental harmonic centered at the operating frequency, while the other harmonics centered at the odd-numbered multiples of the fundamental frequency will be rejected due to the narrow bandwidth. If the transmitted signal is sinusoidal instead, the transmitted power will be the same of the total consumed power since the sinusoidal has only one harmonic to pass through the system and there is no other harmonics attenuated. As a result, at the same transmitted power, the system with the two shapes of transmitted signal will have the same communication distance but with different total consumed power. In the case of sinusoidal, the total power consumed from the source is the same as transmitted power. While in the case of square wave, it is equal to the transmitted power plus the power of the rejected harmonics. As a conclusion, the same transmitted power of a narrow bandwidth NFMIC system with different shapes of transmitted signal could result in the same communication distance at different power consumption.

To study this experimentally, two different shapes of transmitted signal, sinusoidal and square waves, were tested on System#1. The signals were tested almost at the same transmitted power about 369.7 μW. This power was set to this value by adjusting the amplitude of the sinusoidal and square waves and it was calculated using (2.14). The result as shown in Figure 4.5 indicates that the communication distance of the two cases is about the same.

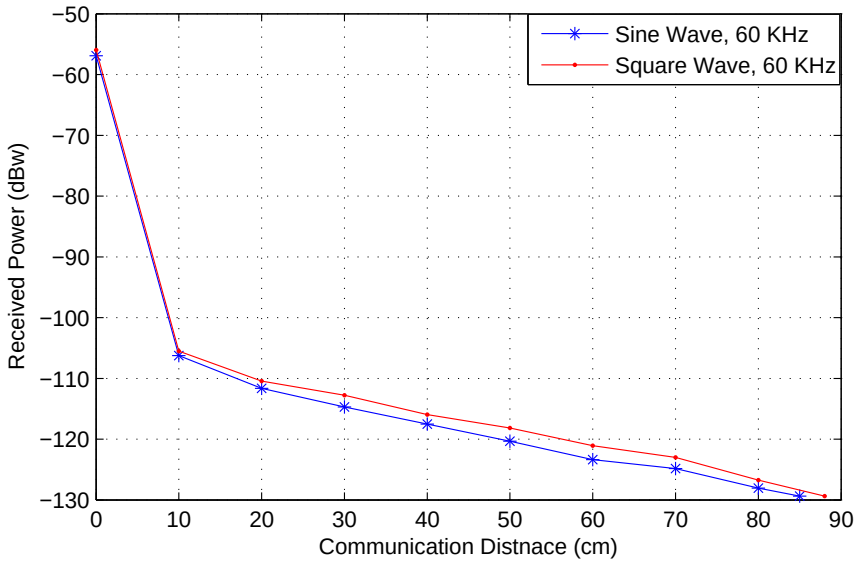

Figure 4.5: Plot of the received power versus communication distance for System#1 when the transmitted signal is a sine wave and when the transmitted signal is square wave

This is expected since the system in the two cases has almost the same transmitted power. However, at this same transmitted power, the system has different power consumed from the source. The consumed power in the case of sinusoidal is equal to the transmitted power which is 369.7 μW. While in the case of square wave, it is equal to the transmitted power plus the power of the other harmonics rejected due to the narrow bandwidth of the system. The bandwidth of System#1 is about 2.2 KHz at operating frequency 60 KHz. This bandwidth can only pass the fundamental harmonic of the square wave centered at the operating frequency and rejects the other odd integer harmonics centered at 180 KHz, 300 KHz, etc. This rejection of harmonics causes the difference between the transmitted power and the total consumed power in the case of square wave compared to the sinusoidal wave. If the total consumed power in the case of square wave is applied on the system when the signal is sinusoidal, its transmitted power will be higher, and thus the communication distance will be higher as well. Finally, matching the spectral characteristics of the transmitted signal to the frequency response of the channel and the transmit/receive filters (including antennas) is a standard communication problem. This problem could be an area for future research to determine the optimal TX signal design to maximize energy efficiency in NFMIC systems.

4.3 Operating Frequency

Based on (2.4) and (2.11), the strength of the magnetic field generated by the TX coil and the amplitude of the induced voltage produced across the RX coil are a linear function of operating frequency. This does not mean that increasing the operating frequency will increase the strength of the magnetic field or the amplitude of the induced voltage of the same NFMIC system. Rather, it means that the strength of the magnetic field and the amplitude of the induced voltage increase as the operating frequency increases until it reaches the resonant frequency, at which the two values will be maximized and beyond which they will start decreasing. The reason for this behavior is related to the relationship between the current, which passes through the TX coil, and the operating frequency. As can be seen from (2.12), this current is maximized when the system operates at the resonant frequency and it starts decreasing as the operating frequency shifts away from it. This behavior causes the relationship we mentioned earlier between the operating frequency and the strength of magnetic field, and between the operating frequency and the amplitude of induced voltage. In conclusion, operating an NFMIC system at resonant frequency is required to maximize the strength of the magnetic field and the amplitude of the induced voltage. Maximizing these two values leads to the highest communication distance.

Figure 4.6 shows the communication distances of System#1 at different frequencies of a sinusoidal voltage signal. The figure illustrates that the communication range of the system increases until approaching the resonant frequency 60 KHz, at which the maximum range occurs, and above which the communication range decreases as frequency increases. This explains that the maximum communication range of any NFMIC system occurs at the resonant frequency. However, this might raise a question: would the communication range increase if the capacitor size is decreased so that the resonant frequency increases? The answer is that each coil has a designated optimal frequency range. Using the coil beyond this range decreases the coils' performance and leads to smaller communication distance. So, the optimum way to get the maximum communication range of any NFMIC system is resonating it in this frequency range. For those coils that we ordered, the frequency range was supplied by the coils' manufacturers. For the coils we wound, it was determined by

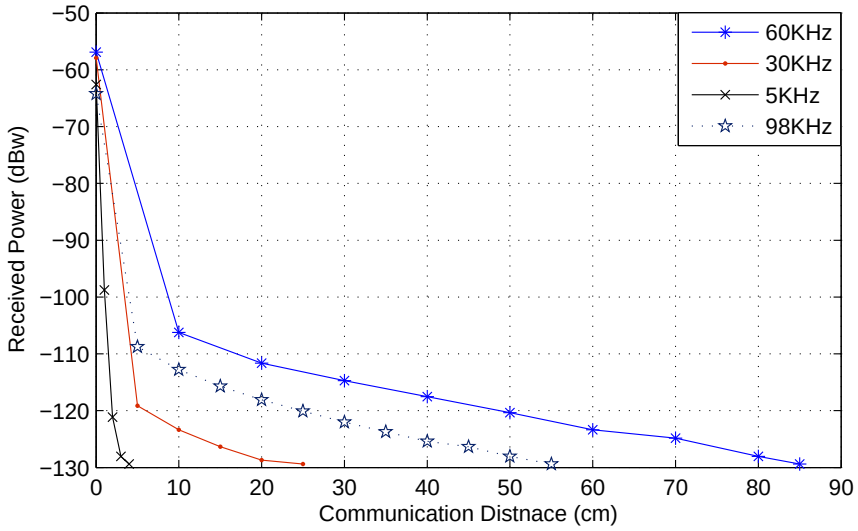

Figure 4.6: Plot of the received power versus communication distance for System#1 at different frequencies

testing.

4.4 Transmitter and Receiver Circuits with Different Coils

Although we do not know exactly how many turns there are in the T-Coils shown in Table 4.1, we know that they have between 3,500 to 33,000 turns. Also, we know that TC_5, 4, 3, 2, and 1 have decreasing number of turns in that order. Using this information and the fact that the magnetic field strength of a coil increases with increasing number of turns, we decided to keep TC_1 as a receiver antenna and change the transmitter antenna as in systems number 1, 2, 3 and 5 shown in Table 4.2. This was intended to increase the magnetic field strength produced by the TX coil in order to make the magnetic bubble size bigger and get a larger communication range.

The result of this approach is shown in Figure 4.7. All the systems achieved almost the same communication distance but at different transmitted power. In the case of System#1, the maximum communication distance was 85 cm at transmitted power 369.7 μW. While in systems 2, 3, and 5, the maximum communication distance was 90 cm at transmitted power

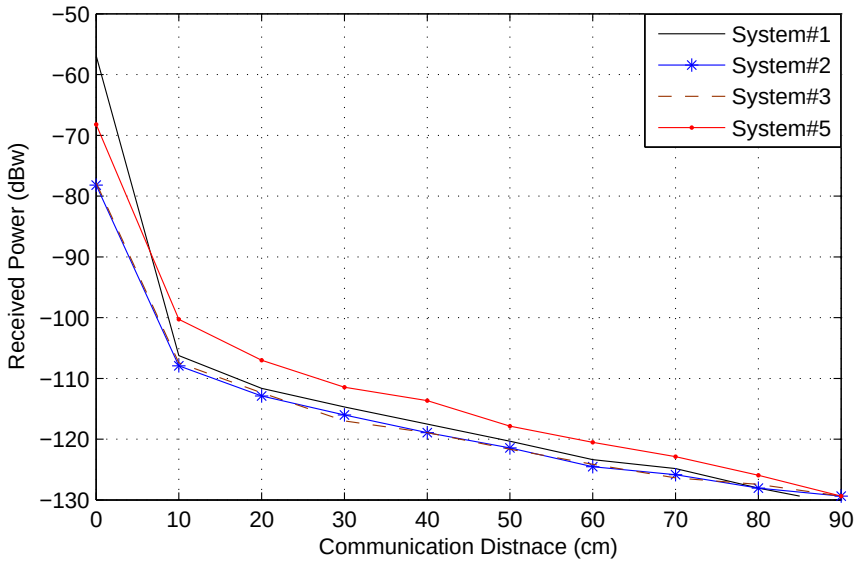

Figure 4.7: Plot of the received power versus communication distance for Systems#1,2,3 and 5.

249.7, 131.5, and 19 μW, respectively, where the transmitted power of the systems was calculated as described in Section 2.3. These results show that the purpose of using different TX coils is achieved when the transmitted power decreases over different systems at the same communication distance. Also, they show that System#5 is the best among these four systems since the transmitted power was the lowest and the communication range was not the smallest. However, the approach has a disadvantage that the bandwidth provided by the system decreases when we use coils with higher inductances relative to their DC resistances in the transmitter circuit as we will explain in Section 4.5.

The same approach was repeated in System#4 and 6. As described in Table 4.2, the transmitter coils in these two systems are the same transmitter coils in System#3 and 5, respectively, while the receiver coil is TC_2 rather than TC_1. According to the manufacturing company, this receiver coil has a higher number of turns and higher sensitivity than TC_1 used in the previous systems; System#1, 2, 3 and 5. This makes System#4 have a higher communication distance than System#3, and System#6 has a higher communication distance than System#5, although they have the same transmitter circuit and transmitted power. We can notice this result from Figures 4.7 and 4.8. From the figures, the maximum

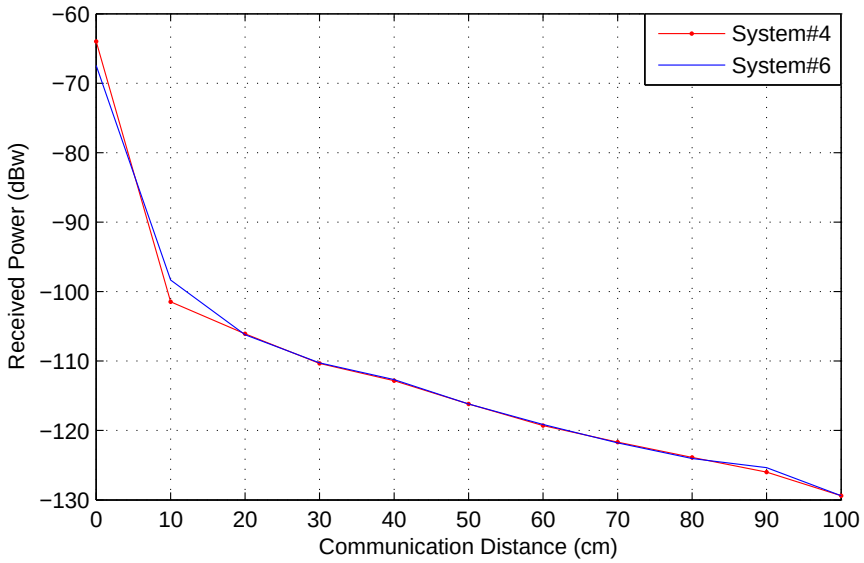

Figure 4.8: Plot of the received power versus communication distance for Systems#4 and 6.

communication distance for System#4 and System#3 is 90 cm and 100 cm respectively at transmitted power of 131.5 μW. As for System#5 and System#6, the maximum communication distance is also 90 cm and 100 cm respectively at a transmitted power of 19 μW.

4.5 Bandwidth Reduction

In Section 4.4, using a coil with a higher number of turns in the transmitter was required to extend the size of the magnetic bubble in order to increase the communication range of an NFMIC system. However, this made the bandwidth provided by the system narrower due to the higher inductance of the coil relative to its DC resistance. In System#1, when the TX antenna was TC_1, the bandwidth provided by the system was approximately 2.2 KHz using (2.25). In System#2 and System#3 where the TX antenna was TC_3 and TC_4 (having higher inductances relative to their DC resistances), the bandwidth of the two systems decreased to about 0.5 KHz and 0.7 KHz, respectively. This indicates that the approach which was followed in Section 4.4 was effective in order to extend the communication range of NFMIC systems, but it reduced the system bandwidth. At the end, we can note that the

bandwidth should be taken into consideration besides transmitted power and communication distance, since they can be improved at the expense of the bandwidth. In regards to the future of work, this will reduce the data transfer rate of the system.

4.6 Transmitted Power versus Maximum Communication Distance

It is well known for any communication system that its communication range increases as the transmitted power increases. The amount of increase differs from one system to another based on the communication scheme. In NFMIC systems, the communication range increases exponentially as the transmitted power increases. Figure 4.9 shows this relation between the transmitted power and communication range. From the figure we can notice that the two systems, System#5 and System#6, have better power performance than the other four systems. This is because of the better TX coil these two systems have compared to the TX coil in the other four systems. The TX coil in these two systems has a higher number of turns which increases the strength of the magnetic field which in turn makes the maximum communication distance longer. In addition, the coil has higher DC resistance that drains lower current from the source which results in lower transmitted power.

The transmitted power shown in Figure 4.9 represents the theoretical transmitted power of the systems calculated as explained in Section 2.3. In Figure 4.10, the transmitted power represents the experimental transmitted power of the system measured as explained in Section 3.2. As we mentioned in this section, the value of resistance R connected in series with the TX coil is different from one system to another depending on the DC resistance of the TX coil. In the systems where the TX coil is TC_1, the value of resistance R is about 10 Ω, while in the other systems when the TX coil is TC_3, TC_4, and TC_5, the value of resistance R is about 50 Ω, 100 Ω, and 1 KΩ, respectively.

From the two figures, it is clear that the theoretical transmitted power is higher than the experimental transmitted power for all systems at all communication distances. As an example in System#1, the theoretical transmitted power at a communication distance of

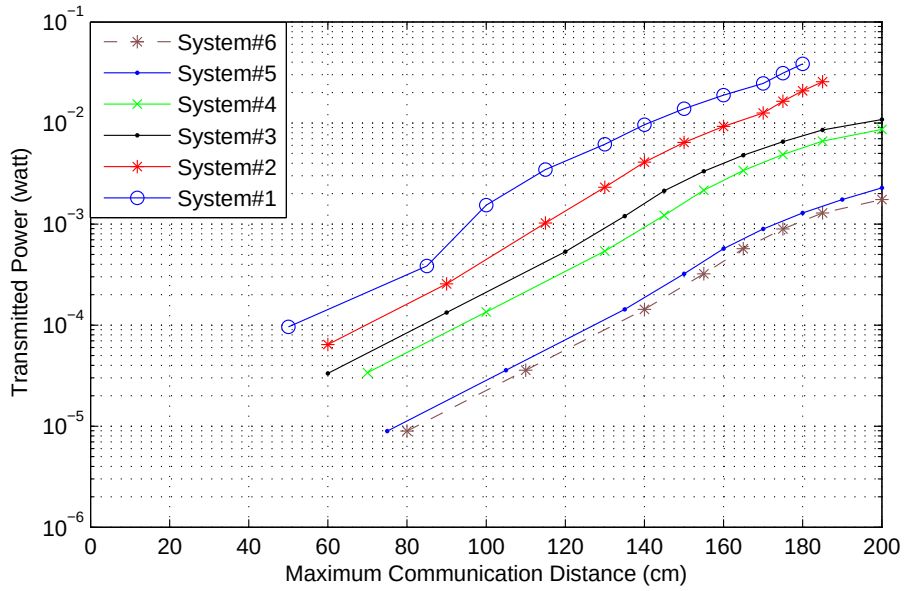

Figure 4.9: Plot of the theoretical transmitted power versus maximum communication distance for the all systems shown in Table 4.2.

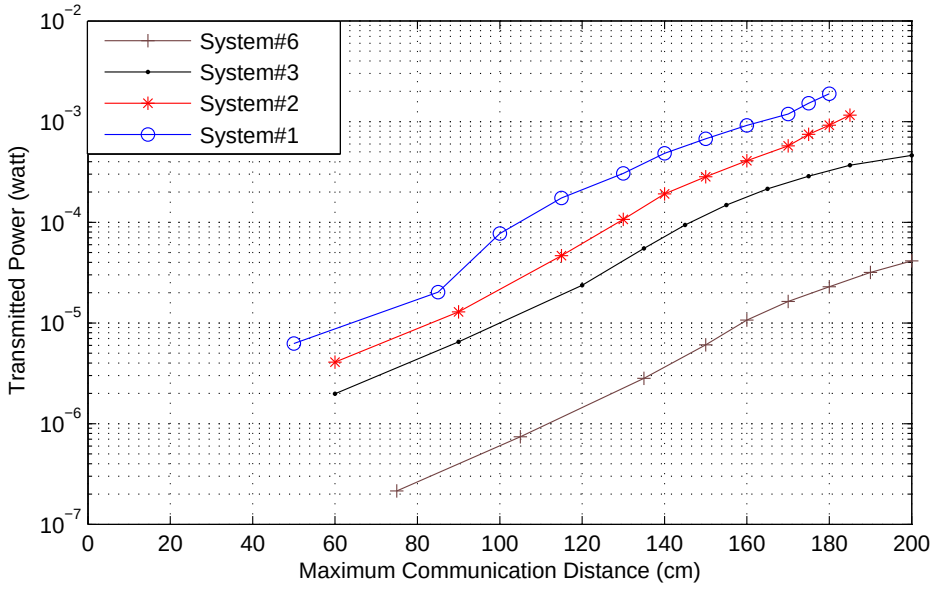

Figure 4.10: Plot of the experimental transmitted power versus maximum communication distance for Systems#1,2,3 and 6.

85 cm is approximately 369.7 μW, while the experimental transmitted power at the same distance is approximately 20 μW, i.e. the theoretical transmitted power of the system is approximately 18.5 times the experimental transmitted power. This means that the value of $i_{1(rms)}$ calculated theoretically is about 4.3 times the $i_{1(rms)}$ calculated experimentally. We believe that this difference between the theoretical and experimental values is because of two reasons. Firstly, the TX circuit is not operating at the resonant frequency. This makes the current $i_{1(rms)}$ that passes through the TX circuit not maximized which in turn makes the transmitted power lower than the actual value. Secondly, the addition of the resistor R to the TX circuit, in order to calculate the experimental transmitted power, makes the current $i_{1(rms)}$ lower than its actual value which as a result makes the transmitted power lower than its actual value as well. At the end, we want to note that the error which occurs by the addition of resistor R is very small. It is equal to 1%, 1.7%, 2.7%, and 7% in the systems when the TX coil is TC_1, TC_3, TC_4, and TC_5, respectively. As a result, it can be considered that the first reason is the main reason of the difference between the theoretical and experimental values of the transmitted power.

Chapter 5

Effect of Obstacles on NFMIC Systems

It was not the primary objective of this project to test the effect of obstacles on NFMIC systems. However, while performing the experiments and taking some measurements, it was noticed that the received signal of the system is affected by our bodies when we stand close to it. This phenomenon motivated us to explore the effect of some barriers like wood, wall, cardboard, concrete, and metal on such systems. We tested all of these materials as barriers between the TX and RX antennas on the same NFMIC system at different communication distances. The test was performed in the Lab shown in Figure 5.1. The Lab contains many reflecting objects, however, the only reflecting objects that feasible within 90 cm, the communication range or the bubble size of the system without barrier, are a computer desk, floor, and two chairs that carry the TX and RX circuits. The result of the test can be classified into three categories. The first category includes barriers that do not have an effect on the system. The second category includes the barrier that has a negative effect on the system and it attenuates the received signal. The last category includes the barriers that have a positive effect on the system and they improve the received signal. The characteristics of these categories will be shown and explained more in the following sections.

Figure 5.1: A view to the Lab where the experiments were performed.

5.1 Category I

This category of barriers has no effect on the NFMIC system. It includes a wooden box, cardboard, and combined cardboard and wooden box. The barriers were tested on System#3. The way of testing these barriers on the system was different from one barrier to another. As for the wooden box, a cubical box with about 0.5 m side length as shown in Figure 5.2 was used. The transmitter circuit was placed inside the box while the receiver circuit was placed outside. So, the transmitter and the receiver circuits were completely isolated from each other. The result is shown in Figure 5.3, where the two curves are almost identical. This means that there is almost no effect of the barriers on the received signal and the communication range of the system. In the case of cardboard, a rectangular cardboard with edges 1 m $\times$ 0.5 m was placed between the transmitter and the receiver. As you can see from Figure 5.3, the curve when the barrier exists is almost identical to the curve when there is no barrier. That means the received signal and the communication distance in both cases are almost the same and the barrier has no effect.

Figure 5.2: The wooden box with about 0.5 m side length that was used in the experiment.

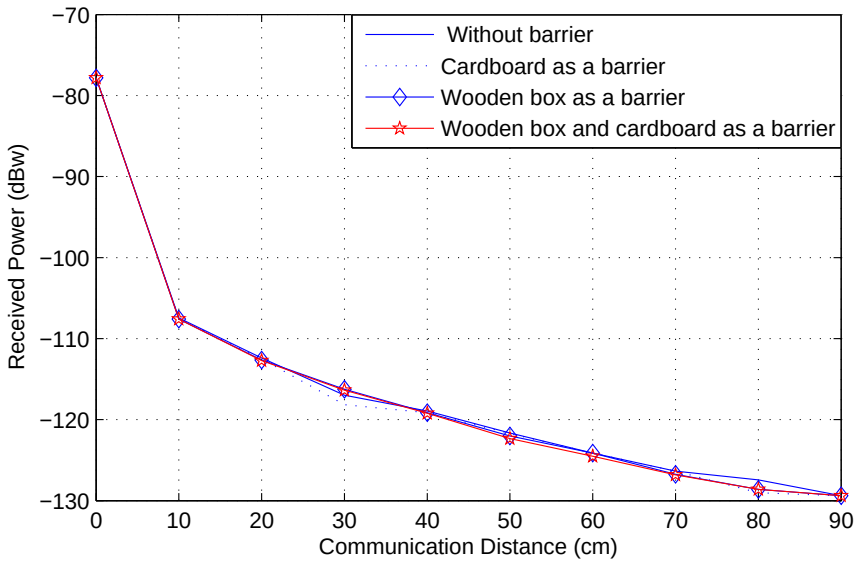

Figure 5.3: Plot of the received power versus communication distance for System#3 with the barriers; wooden box, cardboard, and combined cardboard and wooden box.

In another experiment, the two barriers were tested together at once on the system. In the experiment, the transmitter circuit was placed inside the box while the receiver was placed outside and the cardboard was placed in the middle between them. The result of the experiment shows that the system is unaffected. This is observed from Figure 5.3 where the received signal of the system is approximately the same in both cases with and without barrier. This emphasizes that both the wooden box and cardboard barriers have no effect on an NFMIC system.

5.2 Category II

As mentioned earlier, category II includes the barrier that affects the system and attenuates the received signal. This barrier is a wall. Its thickness was about 12 to 14 cm and it was built out of cinder block. In the experiment, the TX and RX circuits were placed on opposite sides of this wall. This makes both of the circuits completely separated from each other. As a result of this test, Figure 5.4 shows that the communication range of the system is decreased by 20 cm. This attenuating effect of the wall on the system was unexpected. The expected result was to get the same communication range since magnetic field lines have the ability to penetrate objects.

5.3 Category III

This category includes two types of barriers; a metal box and concrete box. These two barriers have a positive effect on the NFMIC system and they were tested on the same NFMIC system used in the first two categories. In two separate experiments, the two barriers were each tested by placing the RX circuit inside the box while the TX circuit outside. Figure 5.5 shows the metal and concrete boxes that were used in this test.

The result of the experiments indicate that the received power of the signal in the case of a barrier is higher than in its absence. This of course makes the communication distance of the system higher as shown in Figure 5.6. In the normal case when no barrier exists, the communication distance is approximately 90 cm. This is 10 cm lower than when there

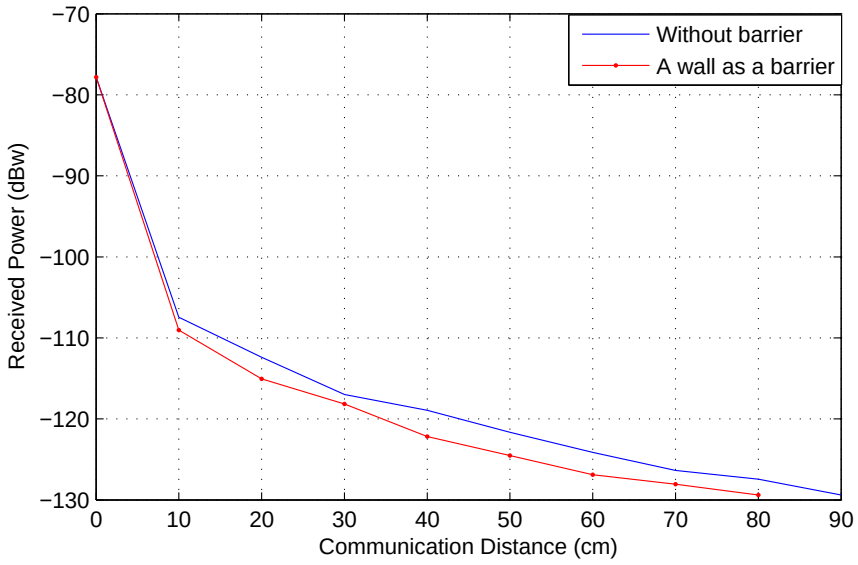

Figure 5.4: Plot of the received power versus communication distance for System#3 with a wall as a barrier.

is metal barrier. When the metal box is replaced with the concrete box, the communication distance extends to approximately 115 cm. These results can be explained by the fact that these barriers' permeability are higher than the permeability of the surrounding air. From (2.19), a medium with higher permeability results in higher received power and communication range.

In conclusion, we learn from this chapter that any barrier isolating the transmitter from the receiver or placed close to one of them may or may not have an effect on NFMIC systems. An effect if present may be positive or negative. The attenuation effect of a barrier is determined by its permeability. A barrier with permeability similar to air does not affect magnetic field lines as they pass through them. As for those that have a positive effect, these barriers have permeability higher than the permeability of air. Thus, they increase the magnetic field strength according to (2.4), resulting in a higher distance of communication. The opposite holds true for the attenuating barrier, the wall. We have no logical interpretation since we expected that it will have no effect according to the ability of magnetic field lines to penetrate objects. Finally, these experiments open the door in the future to test more types of barriers. For example, testing different types of concretes and

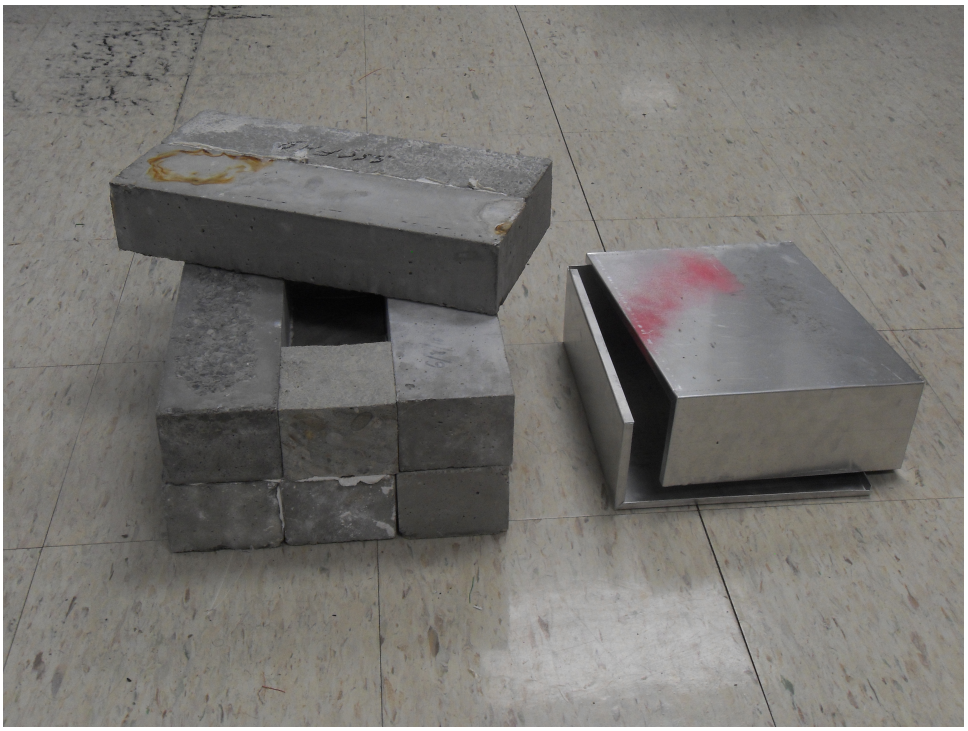

Figure 5.5: The metal and concrete boxes that were used in the experiment.

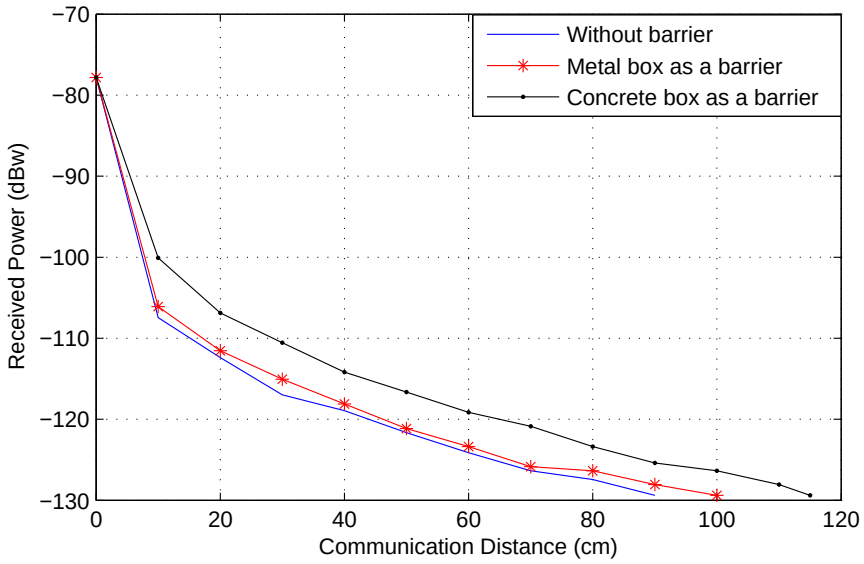

Figure 5.6: Plot of the received power versus communication distance for System#3 with the barriers; metal box and concrete box.

testing the human body since each organ has different specific absorption rate (SAR) [24]. In addition, the experiments turn out that it might be a good idea to use near field magnetic induction communications in concrete-embedded sensors, especially, in the application of monitoring the health of concrete in bridges and buildings.

Chapter 6

Wakeup Application

In wireless sensor networks, the energy consumption of nodes can be reduced by reducing the duration of their idle listening time. Reducing this duration of time can be implemented using methods such as periodically listening on the radio channel. This method requires the transmitter to send a wakeup signal in order to inform its neighbors of impending data transfer. If lower wakeup signal energy was used in such a method, the energy consumption of nodes would be further saved. This work is aimed to this purpose, which is reducing the energy of wakeup signal, using NFMIC technology. The idea of using this technology for this purpose came out of the property that NFMIC technology can communicate wirelessly using low power. At the end, reducing the energy of wakeup signal will extend the lifetime of nodes in dense sensor networks, specially, in embedded sensor network in the concrete since the results in Section 5.3 shows that concrete has positive effect on NFMIC systems.

In this chapter, after optimizing our NFMIC system in chapter 4, we will show how the wakeup application was implemented using $TelosB$ mote as a node. We will show the system overview that illustrates the way in which the node is interfaced to an NFMIC system. At the end, we will show the way we compute the wake-up energy and the results for this energy versus distance.

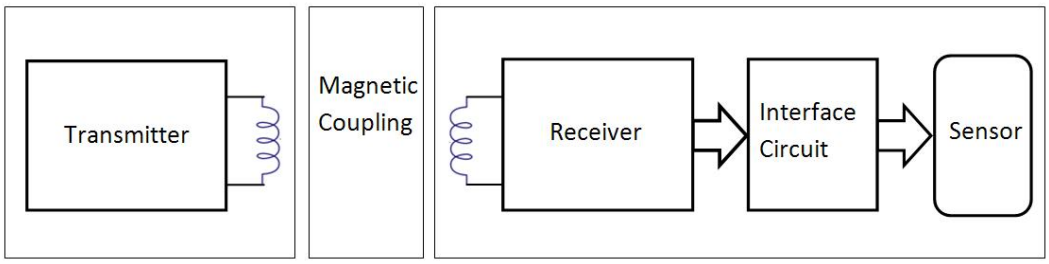

Figure 6.1: Overall flow diagram for an NFMIC system attaching to a sensor.

6.1 System Overview

The block diagram, shown in Figure 6.1, illustrates the overall system layout in which the near field magnetic induction communication system is attached to the sensor. As for the transmitter block, it has the same circuit shown earlier in Figure 3.1. It is merely a series combination of a function generator, a capacitor and a coil. From this combination, the wake up pulse will be generated and sent over a wireless magnetic link to the receiver. The receiver, which also has the same elements, will receive this wake-up signal and pass it to the sleeping sensor through an interface circuit. The interface circuit makes the decision whether to wake up the sensor or not based on a threshold. This threshold is a DC voltage and it is a little higher than the noise level.

6.2 Interfacing with the Sensor

Attaching the receiver circuit directly to the sensor will not work for waking it up or for saving power for three reasons. First, the impedance between the receiver circuit and the sensor should be matched. Otherwise, there will be loss in the received signal and the signal becomes lower than its actual value and not enough to wake up the sensor. As a result, the sensor will keep sleeping and the data will be lost. Second, the received signal is an AC signal and it has very small amplitude with a value in millivolts. This value is not enough to wake up the sensor since the sensor we are using is a *TelosB* mote and it needs a DC voltage with amplitude of 3 V to wake up. Finally, the noise in the environment always has a signal that can be sensed by the receiver with changeable amplitude. If we use an amplifier

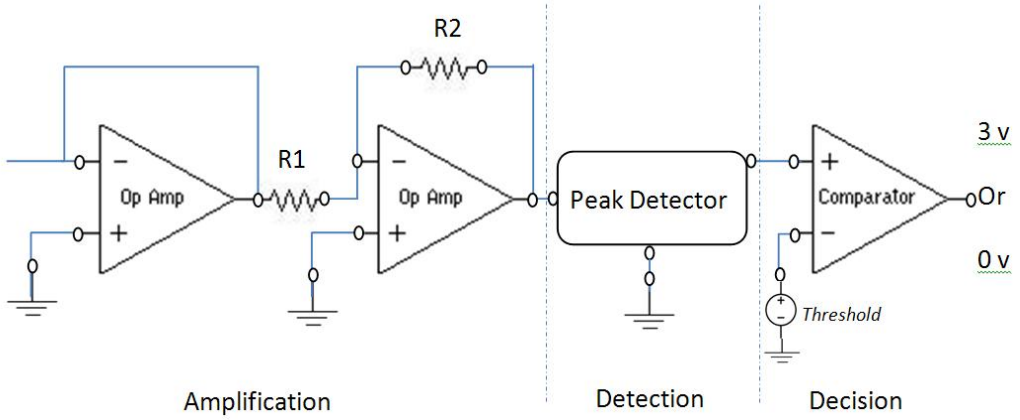

Figure 6.2: Interface circuit between the receiver and sensor.

to amplify the signal as a solution for the second problem, the noise signal is also amplified. This could wake up the mote if there is no threshold to show that any signal level below it is noise. Of course, waking up the sensor due to noise when there is no data is a waste of power.

To avoid these problems, an interface circuit was designed to be connected between the receiver circuit and the sensor. As shown in Figure 6.2, this circuit has three stages; Amplification, Detection, and Decision. The amplification stage has two purposes; the first purpose is to match the output impedance of the receiver circuit with the amplifier. The second purpose is to amplify the signal to be in the range of the signal detector in the next stage. In the detection stage, the amplified signal passes through a signal detector in which the peak value of the signal is detected to be represented as a DC voltage at the output. In the decision stage, the output of the detector will be compared with a threshold. If the detector output is higher than the threshold, the output will be 3 V, which is the voltage required to wake up the sensor. But if the detector output is lower than the threshold, the output will be 0 V and the sensor will remain sleeping. As we mentioned earlier, threshold is a DC voltage and it is a little higher than the noise level. We will discuss these three stages in detail in the following sections.

6.2.1 Amplification Stage

As shown in Figure 6.2, this stage includes two stage cascaded amplifiers in order to achieve the two purposes of matching impedance and amplification. Both these amplifiers are represented using an $LF411CN$ amplifier chip. In the first amplifier, the non-inverting input is connected directly to the output of the receiver circuit, while the other terminal, inverting input, is connected to the output. This method of connection makes it a voltage follower in which the voltage at the input is same as the voltage at the output [25]. This is to avoid the voltage loss which occurs due to the impedance mismatch between the receiver circuit and the second amplifier. In the second amplifier, two resistors R_1, R_2 are added to it as shown in Figure 6.2. The inverting input is connected to the output through a resistor R_2 with size 10 $M\Omega$, while the non-inverting input is connected to the ground. The output of the follower amplifier is connected to the inverting input of the second amplifier through a resistor R_1 of size 1 MΩ. This makes the second amplifier work as an inverting amplifier with gain 10 dB. In conclusion, the amplification stage is really important to be added in the interface circuit for two reasons. Firstly, it is to overcome the problem of impedance mismatch which causes voltage loss that can cause shorter communication distance. Secondly, it is to amplify the small received signal to make it in the range of the V-peak detector to be detected in the next stage.

6.2.2 Detection Stage

The main aim of this stage is to detect any signal in the environment and convert its RMS value to DC value to be ready for comparison in the Decision stage. For this purpose, we used a magnitude detector which is described in [26]. The detector has a 68 dB dynamic range and consumes less than a μW. It has a circuit with two stages that have been fabricated in 0.18 μm and 0.5 μm processes. The output of the first stage tracks the RMS of the input signal, which is the output of the amplification stage, with a significant ripple. This ripple is removed in the second stage of the detector, so the output will only be left with a DC value. This DC value will be passed to the next stage to make a decision about whether to wake up the sensor or not.

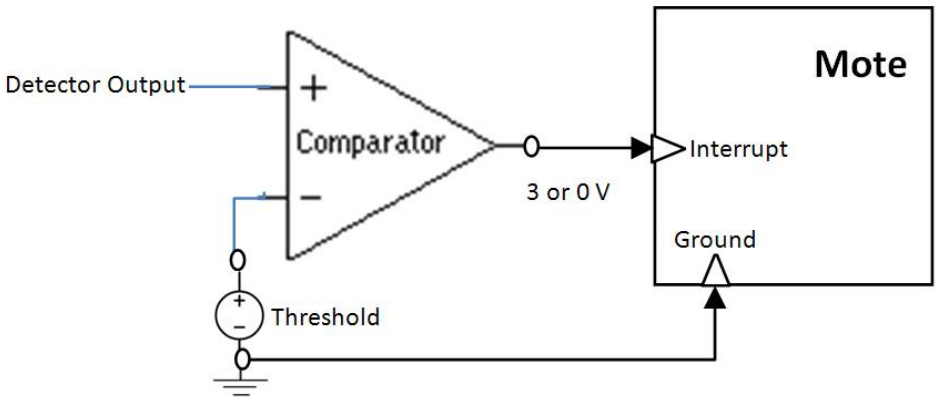

Figure 6.3: Connecting the output of the comparator to the sensor through its interrupt pin.

6.2.3 Decision Stage

In this stage, the decision of waking up the sensor is made based on the comparison between the DC value which comes out from the detector and the threshold. The comparison is performed using an $LM393$ comparator. It is a high gain and wide bandwidth device. It has two input terminals. One of them is connected to the input signal while the other terminal is connected to a DC voltage source as a reference or threshold value. The input signal is the output of the detector in this case. Depending on the result of the comparison, the output of this comparator is either high (V_{cc}) or low (0). If the input signal is higher than the threshold, the output will be equal to the V_{cc} which is adjusted to 3 V, the voltage required for the sensor to wake up. Otherwise, the output will be low which means that there is nothing transmitted and the sensor will stay in sleeping mode.

6.3 TELOS MOTE

The sensor which was used for the wake up application was $TelosB$ mote [27]. This mote has been chosen for its wide use, low-power sleep mode, and fast wake up time. The mote was attached to the last stage of the interface circuit as illustrated in Figure 6.3. The output of the comparator is directly connected to the interrupt-enabled general I/O pin of the mote. Through this pin, the mote is interrupted to switch from sleep mode to wake-up mode, where the interruption occurs whenever the output of the comparator transitions from

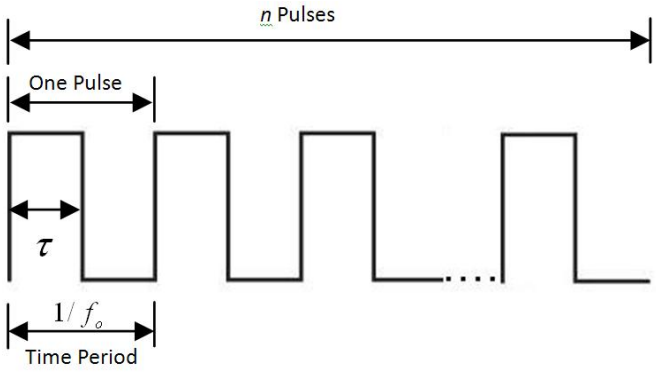

Figure 6.4: The shape of the pulses sequence that are transmitted to wake up the mote.

low to high, i.e. from 0 V to 3 V. As a flag to prove that the mote switches to the wake-up mode, a TinyOS application program was installed in the mote to turn on the LEDs for 500 ms for each interruption. When the interruption occurs, every part in the mote turns on including the microprocessor. In turn, the microprocessor runs the program to turn the LEDs on for 500 ms. The program is included in Appendix (A.1) showing all the components and interfaces which are needed to implement the application.

6.4 Wake-Up Energy

Wake-Up Energy is the energy required to be transmitted from a particular distance to wake up the sleeping mote. This amount of energy increases as the communication distance increases. It is computed by multiplying the transmitted power by the time needed for the signal to be transmitted. In our case, as shown in Figure 6.4, the transmitted signal is a sequence of pulses where each pulse has an amplitude of 15 Vp-p and a duty cycle of 50%. The pulse is equal to the half of the time period that represents the inverse of operating frequency. The time for which the pulses are being transmitted is equal to the width of a single pulse times the number of pulses. If we consider that f represents the operating frequency of the system, the width of a single pulse τ can be given as

$$\tau = \frac{1}{2f} \qquad \text{Sec.} \tag{6.1}$$

The energy which is consumed by one pulse can be calculated as

$$E_p = \int_0^{\tau} P_{TX} \cdot dt \qquad \text{J.} \tag{6.2}$$

Using (2.14), (6.2) can be expressed as

$$E_p = \int_0^{\tau} {i_1}^2{}_{(rms)} \cdot R_{L1} \cdot dt. \tag{6.3}$$

Both of $i_{1(rms)}$ and R_{L1} are not a function of time. So, the equation can be rewritten as

$$E_p = ({i_1}^2{}_{(rms)} \cdot R_{L1}) \cdot \tau. \tag{6.4}$$

Equation (6.4) represents the energy in *Joules* (J) consumed by one pulse. In the case when we have a sequence of pulses with a number n, the total consumed energy for these pulses can be calculated as

$$E = ({i_1}^2{}_{(rms)} \cdot R_{L1}) \cdot \tau \cdot n \qquad \text{J,} \tag{6.5}$$

where, the term $\tau \cdot n$ represents the total time along which the pulses are being transmitted to wake up the mote. The number of pulses increases as the communication distance increases. Of course, this means that the consumed energy increases as the communication distance increases as well. This relationship between the energy required for waking up the mote and communication distance of the system is explained in detail in the next section.

6.4.1 Wake-Up Energy versus Communication Distance

This section presents the results showing the relationship between the amount of energy required for waking up the mote and the communication distance of the system. The results were taken for the three NFMIC systems: System#3, System#4, and System#6, where each system has a different combination of TX and RX antenna coils. At different distances from the transmitter, we determined the number of pulses that are required to be transmitted to wake up the mote at the receiver side. Based on these numbers and using (6.5), we calculate the wake-up energy at these different locations. Table 6.1 shows the number of pulses required to be transmitted for waking up the mote to the three systems at different locations. In the table, the number at which the system type and any of the distances are

intersected at represents the number of transmitted pulses required for waking up the mote at that distance.

In order to calculate the wake-up energy consumed by each system with respect to the corresponding communication distance, we calculated the energy consumed by one pulse and then multiplied it by the number of pulses required for waking-up at that distance. In the case of System#3, the energy consumed by a single pulse was 451.66 pJ. While in the case of the two systems, System#4 and System#6, it was 749.7 pJ and 72.8 pJ, respectively. Using these single pule energies, the wakeup energy of the three systems can be calculated at any distance. For example, at distance 90 cm where the number of pulses required for waking up is 30000, 11000, 15000, respectively as shown in Table 6.1, the wakeup energy of the three systems is approximately 13.5 μJ, 8.2 μJ, and 1.1 μJ, respectively. If the energy source in the three systems is an AA battery (Akaline Long-Life with energy 9360 J) [28], the total number of wakeup signals that could be transmitted by these systems will be approximately 9 Billion, 2 Billion, and 1.5 Billion wakeup signals, respectively.

System	10cm	20cm	30cm	40cm	50cm	60cm	70cm	80cm	90cm	100cm
System#3	2	4	8	14	70	600	1600	2500	30000	$\succ$ 50000
System#4	1	2	4	7	15	50	500	1200	11000	50000
System#6	1	2	5	8	12	50	500	100	15000	40000

Table 6.1: The number of pulses which were need to wake up the mote at different communication distances for Systems#3,4 and 6. These measurements were taken at noise level 2.08mV

As seen earlier, the consumed energy per pulse for System#4 is higher than the consumed energy per pulse for System#3, although it has better energy efficiency as shown in Figure 6.5. This is because at the same communication distance, System#3 needs a higher number of pulses to wake up the mote than System#4 as shown in Table 6.1. As for System#4 and System#6, from the table, it can be noticed that the number of pulses required in the case of System#4 is either equal or relatively close to the number of pulses required in the case of System#6. This does not reflect their energy efficiency shown in Figure 6.5, where the curves are not identical or not even very close to each other. The reason is related to the

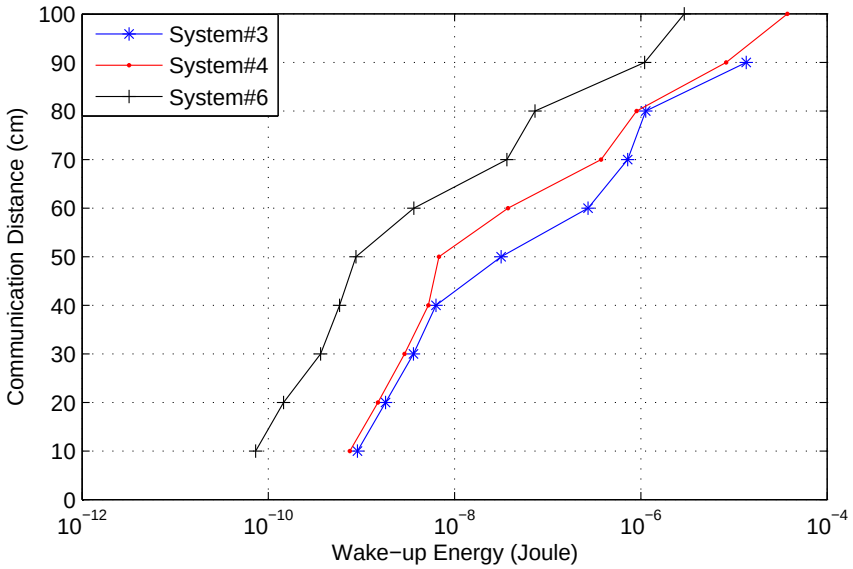

Figure 6.5: Wake-up energy versus communication distance for the three systems; System#3, System#4, and System#6

amount of energy which is consumed per pulse for each system. The energy consumed per pulse for System#6 is approximately 10 times the energy consumed per pulse for System#4 which makes the curves different from each other. At the end, we want to note that the energy consumed per pulse for System#3 was calculated when the operating frequency of the system was 100 KHz and the pulse width was 5 μs. In the System#4 and System#6, it was calculated when the operating frequency was about 60 KHz and the pulse width was 8.33 μs. In addition, the amplitude of the pulses coming out from the source for the three systems was 15 $Vp-p$.

6.4.2 Wake-Up Energy versus Communication Distance at Different Noise Levels

Wake-up energy depends on the noise level in the environment. It increases as the noise level increases. When the noise level increases, this forces us to increase the threshold value of the comparator to avoid interrupting the mote due to the noise. Of course, increasing the threshold needs higher transmitted energy to exceed it in order to wake up the mote. Figure 6.6 shows three curves for the wake-up energy versus distance that were plotted at different

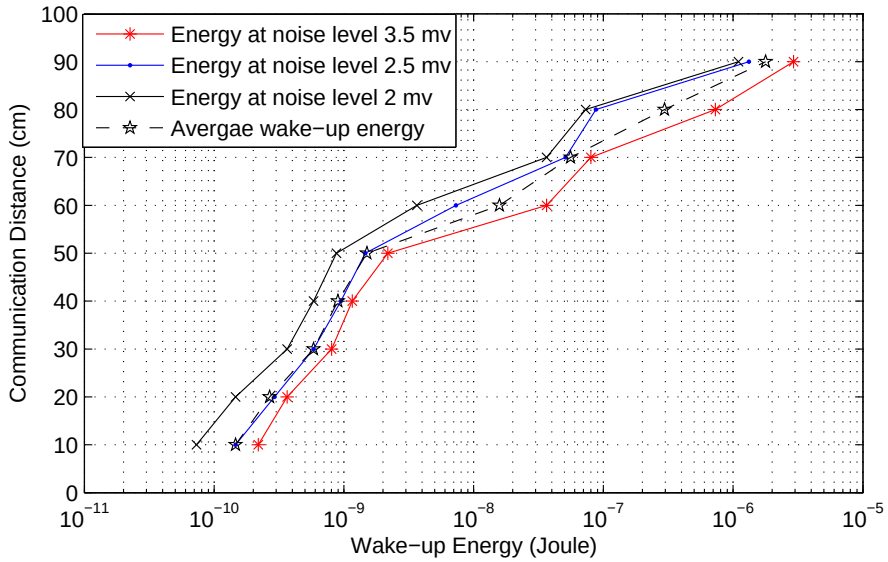

Figure 6.6: Wake-up energy versus communication distance for System#6 at three different noise levels

noise levels for System#6.

From the figure, we can notice that at the same communication distance for the three curves, the energy increases as the noise level increases. For example, at the distance 90 cm, the energy increases from about 1 μJ to about 1.5 μJ when the average noise level increases from about 2 mV to about 2.5 mV. It increases more to reach about 3 μJ when the average noise level increases to about 3.5 mV. This reinforces the fact that increasing the noise in the environment makes the energy required for waking up the mote higher. Finally, the dashed curve in the figure represents the average wake-up energy for the three cases of noise level. For example, at distance 90 cm, the average wake up energy for the three curves is about 2 μJ.

6.5 Results

In this work, the minimum energy required for waking-up a node was 1.1 μJ, the wakeup energy achieved by System#6. This energy represents only the energy consumed by the transmit circuit and does not include the energy consumed by the receive side. This energy is very small compared to the energy consumed by the transmit node in the B-MAC protocol.

In this common protocol, the energy consumed by the transmit node is equal to the duration time of preamble (channel check interval) times the transmitted power. In the typical values of the CC2420 radio [29] which is used in Telosb motes, the transmitted power is 52.2 mW. Since the optimum length of a preamble in B-MAC in a wireless network with 2 nodes is about 100 ms [30], the energy consumed by the TX node using this protocol is 5.22 mJ. This amount of energy is very high compared to 1.1 μJ, the energy that was calculated in System#6.

If the energy consumed by the receive side is taken into consideration, the total energy (TX and RX energy) of our system per wakeup will be higher than the total energy consumed by the B-MAC protocol per wakeup. In the case of B-MAC, the energy consumed by the receive node is equal to the time duration of polling the channel times the power in receiving. Using the typical values of CC2420 radio, the power in receiving is 12.3 mW and the polling duration time is 2.5 ms. From this, the energy consumed by the receive node is 30.075 μJ, and thus the total consumed energy per wake up is 5.25 mJ. In the case of System#6, the energy consumed by the receiver is equal to the energy consumed by the interface circuit. This energy is equal to the power consumed by each stage times the total time along which the pulses are being transmitted. The power consumed in the three stages; amplification, detection, and comparison is 32.4 mW, 2.4 mW, and 1 μW, respectively. Since the total time along which the pulses are being transmitted in System#6 is 8.33 μs, the energy consumed by the receiver is 11.401 mJ, and thus the total energy consumed per wakeup is 11.402 mJ.

This high amount of energy consumed by our system compared to the B-MAC protocol is due to the high energy consumed by the receive circuit. In this work, we did not work on the receiver to minimize its consumed power since our primary objective was minimizing the power required for waking up. This result of comparison opens the door for two areas of research in future. The first area of research is optimizing the receiver circuit of an NFMIC system in order to reduce its consumed power. The second area is using NFMIC technology with B-MAC protocol rather than CC2420 radio to get low consumed power in both of TX and RX sides.

Chapter 7

Conclusions

7.1 Summary and Conclusions

In this thesis, we took the advantage of NFMIC technology to achieve the goal of low power wake-up signaling for dense sensor networks. Using the coils we have, we first optimized our NFMIC system based on power efficiency. We then implemented our wakeup application and calculated the energy consumed per wake-up. This energy was computed with respect to the distance at which the sensor is placed from the transmitter. As a result, we can conclude that the amount of energy consumed per wake-up depends on the physical specifications of the TX and RX coils, in particular, the number of turns. The higher is number of turns, the lower is the energy consumed per wake-up. This fact was shown in Section 7.5 using the three systems: System#6, System#4, and System#3. The coils in System#6 have higher number of turns than the coils in System#4, and the coils in System#4 have higher number of turns than the coils in System#3. The energy consumed per wake-up by each system was 1.1 μJ, 8.24 μJ, and 13.5 μJ respectively when the sensor was placed at a distance of 90 cm from the transmitter. In addition, the energy depends on the noise level in the environment. For System#6 and at a distance of 90 cm, the energy was calculated at three different noise levels 2 mV, 2.5 mV and 3.5 mV and the result was about 1 μJ, 1.5 μJ, and 3 μJ, respectively. This indicates that the energy required per wake up increases as the noise level increases. Finally, we can also conclude from this work that obstacles may or may not affect NFMIC systems. An attenuation effect, if present, may be positive or negative

and it is determined by the barrier's permeability.

7.2 Future Work

In the future, we plan to improve the energy efficiency that is achieved in this work. This could be implemented using different coils that have a higher sensitivity and generate a stronger magnetic field. These two factors can be improved depending on the coils' specifications. For this task, we intend to use some different RFID coils. As another approach, we will recalculate the wake-up energy in the presence of obstacles. This could be done for the obstacles that already have been tested in this work. In addition, as a future work, we will try to determine the optimal TX signal design that maximizes energy efficiency in NFMIC systems since some forms of TX signal might cause loss in energy as discussed in Section 4.2. Also, we plan to do some experiments on NFMIC technology as an ultra-low power communications technology. In this, we will look at high data rate communications with the goal of improving the power efficiency with respect to the communication distance. Finally, we will work on optimizing the receiver circuit to minimize its power consumption, and we plan to use NFMIC technology with B-MAC protocol rather than CC2420 radio to get low consumed power in both of TX and RX sides.

Appendix A

TinyOS Program

A.1 Wake-up Application using TinyOS

The application is a TinyOS program that calls a timer to turn the LEDs on for 500 ms for each interruption. The application is composed of two components: a module, called "Wakeup.nc", and a configuration, called "WakeupAppC.nc". The configuration file provides the components that provides the interfaces which are used in the module file. Using these components and interfaces, the application makes the *TlosB* mote blinks for 500 ms for any interruption.

```
configuration WakeupAppC{
}
implementation {
components MainC, WakeupApp;
WakeupApp -> MainC.Boot;
/********** Leds **************/
components LedsC;
WakeupApp.Leds -> LedsC;
/******** Timer ************/
components new TimerMilliC() as TimerSettings;
WakeupApp.TimerSettings -> TimerSettings;
components new TimerMilliC() as TimerEventHoldOff;
WakeupApp.TimerEventHoldOff -> TimerEventHoldOff;
components HplMsp430GeneralIOC;
WakeupApp.eventInt -> HplMsp430GeneralIOC.Port23; // Interrupt Wakeup pin
/********** Interrupt **************/
```

components HplMsp430InterruptC;
WakeupApp.eventInterrupt -> HplMsp430InterruptC.Port23; // GIO3
WakeupApp.eventIntUsr -> HplMsp430InterruptC.Port27; // UserInt
}

module WakeupApp {
uses interface Boot;
/********** Leds **********/
uses interface Leds;
/******** Timer ***********/
uses interface Timer<TMilli> as TimerSettings;
uses interface Timer<TMilli> as TimerEventHoldOff;
/******** Digital I/O **********/
uses interface HplMsp430GeneralIO as eventInt;
/********** Interrupt **********/
uses interface HplMsp430Interrupt as eventInterrupt;
uses interface HplMsp430Interrupt as eventIntUsr;
}
implementation{
*uint*16_*t* currentSupplyVoltage = 0;
*uint*8_*t* eventCount = 0;
bool eventServicing = FALSE;
/*************** Boot ***************/
event void Boot.booted() { // Set pins
call eventInt.makeInput();
call eventInterrupt.enable();
call eventInterrupt.edge(TRUE); // rising edge
call eventIntUsr.enable();
call eventIntUsr.edge(TRUE);
}
/********** Timer ***************/
event void TimerEventHoldOff.fired(){
call eventInterrupt.clear();
call eventInterrupt.enable();
call eventIntUsr.clear();
call eventIntUsr.enable();
}
/************* Interrupt ******************/
async event void eventInterrupt.fired(){
call Leds.led2On();

```
call Leds.led1On();
call Leds.led0On();
call TimerSettings.startOneShot(500);
call eventInterrupt.clear();
}
async event void eventIntUsr.fired(){
call Leds.led2On();
call Leds.led1On();
call Leds.led0On();
call TimerSettings.startOneShot(500);
call eventIntUsr.clear(); }
/********* Begin event response code **********/
event void TimerSettings.fired(){
call Leds.led2Off();
call Leds.led1Off();
call Leds.led0Off();
}
}
```

References

[1] M. Masihpour and J.I. Agbinya, "Cooperative relay in near field magnetic induction: A new technology for embedded medical communication systems," in *Broadband and Biomedical Communications (IB2Com), 2010 Fifth International Conference on*, dec. 2010, pp. 1 –6.

[2] H.G. Schantz, "Near Field Propagation Law & A Novel Fundamental Limit to Antenna Gain Versus Size," in *Antennas and Propagation Society International Symposium, 2005 IEEE*, july 2005, vol. 3A, pp. 237 – 240.

[3] Johnson I. Agbinya, Nithya Selvaraj, Arthur Ollett, Stephane Ibos, Yasmin Ooi-Sanchez, Mark Brennan, and Zenon Chaczko, "Characteristics of the magnetic bubble 'cone of silence' in near-field magnetic induction communications," *BattleField Technology*, vol. 13, no. 1, pp. 21–25, March. 2010.

[4] K. Fotopoulou and B.W. Flynn, "Optimum antenna coil structure for inductive powering of passive rfid tags," *2007. IEEE International Conference on RFID*, pp. 71–77, March. 2007.

[5] R. Bansal, "Near field magnetic communication," *IEEE Antennas and Propagation Magazine*, vol. 46, no. 2, pp. 14–15, April. 2004.

[6] S. Hoskins, T. Sobering, D. Andresen, and S. Warren, "Near-field wireless magnetic link for an ingestible cattle health monitoring pill," *Engineering in Medicine and Biology Society, 2009. EMBC 2009. Annual International Conference of the IEEE*, pp. 5401 –5404, Sept. 2009.

[7] M. Pasquet, J. Reynaud, and C. Rosenberger, "Secure payment with NFC mobile phone in the smarttouch project," in *Collaborative Technologies and Systems, 2008. CTS 2008. International Symposium on*, may 2008, pp. 121 –126.

[8] A. Marcus, G. Davidzon, D. Law, N. Verma, R. Fletcher, A. Khan, and L. Sarmenta, "Using NFC-enabled mobile phones for public health in developing countries," in *Near Field Communication, 2009. NFC '09. First International Workshop on*, feb. 2009, pp. 30 –35.

[9] Joseph Polastre, Jason Hill, and David Culler, "Versatile low power media access for wireless sensor networks," *In Processing of the 2nd ACM SenSys Conference*, pp. 95 – 107, November 2004.

[10] K. J. Wong and D. K. Arvind, "Speckmac: low-power decentralised mac protocols for low data rate transmissions in specknets," *Proceedings of the second international workshop on Multi-hop ad hoc networks: from theory to reality*, pp. 71–78, 2006.

[11] C.R. Nave, "Mutual inductance," *Phy − astr.gsu.edu*. Department of Physics and Astronomy, Georgia State University, Aug.2000. Web. 10 July 2010.≺ http://hyperphysics.phy-astr.gsu.edu/hbase/magnetic/indmut.html#c2 ≻.

[12] H.C. Jing and Y.E. Wang, "Capacity performance of an inductively coupled near field communication system," *Antennas and Propagation Society International Symposium, 2008. AP-S 2008. IEEE*, pp. 1 –4, July 2008.

[13] C.R. Nave, "Ampere's law," *Phy − astr.gsu.edu*. Department of Physics and Astronomy, Georgia State University, Aug.2000. Web. 10 July 2010.≺ http://hyperphysics.phy-astr.gsu.edu/hbase/magnetic/amplaw.html ≻.

[14] C.R. Nave, "Biot-savart law," *Phy − astr.gsu.edu*. Department of Physics and Astronomy, Georgia State University, Aug.2000. Web. 10 July 2010.≺ http://hyperphysics.phy-astr.gsu.edu/hbase/magnetic/biosav.html#c1 ≻.

[15] Michael W. Davidson, "Faraday's magnetic field induction experiment," *micro.magnet.fsu.edu/index.html*. Florida State University, 1995-2010. Web. 20 Sep 2010.≺ http://micro.magnet.fsu.edu/electromag/java/faraday2/ ≻.

[16] C.R. Nave, "Faraday's law," *Phy − astr.gsu.edu*. Department of Physics and Astronomy, Georgia State University, Aug.2000. Web. 10 July 2010.≺ http://hyperphysics.phy-astr.gsu.edu/hbase/electric/farlaw.html#c1 ≻.

[17] C.R. Nave, "Lenz's law," *Phy − astr.gsu.edu*. Department of Physics and Astronomy, Georgia State University, Aug.2000. Web. 10 July 2010.≺ http://hyperphysics.phy-astr.gsu.edu/hbase/electric/farlaw.html#c2 ≻.

[18] D.C. Hogg, "Fun with the friis free-space transmission formula," *Antennas and Propagation Magazine, IEEE*, vol. 35, no. 4, pp. 33 –35, aug 1993.

[19] Mark W. Lund, "Wire Gauge and Current Limits," *http : //www.powerstream.com*. PowerStream Technologies, 2000. Web. 25 Sep 2010.≺ http://www.powerstream.com/Wire_Size.htm ≻.

[20] C.R. Nave, "Selectivity and Q of a Circuit," *Phy − astr.gsu.edu*. Department of Physics and Astronomy, Georgia State University, Aug.2000. Web. 21 Sep 2010.≺ http://hyperphysics.phy-astr.gsu.edu/hbase/electric/serres.html#c3 ≻.

[21] Youbok Lee, "RFID coil design," *Microchip Technology Inc*, , no. AN678, pp. 1 – 18, 1998.

[22] C.R. Nave, "Resonance," *Phy − astr.gsu.edu*. Department of Physics and Astronomy, Georgia State University, Aug.2000. Web. 12 Sep 2010.≺ http://hyperphysics.phy-astr.gsu.edu/hbase/electric/serres.html#c1 ≻.

[23] Eric W Weisstein, "Fourier Series–Square Wave," *mathworld.wolfram.com*. MathWorld–A Wolfram Web Resource, 1999. Web. 25 Sep 2010.≺ http://mathworld.wolfram.com/FourierSeriesSquareWave.html ≻.

[24] S. Cecil, G. Schmid, K. Lamedschwandner, J. Morak, G. Schreier, A. Oberleitner, and M. Bammer, "Numerical assessment of specific absorption rate in the human body caused by nfc devices," *Near Field Communication (NFC), 2010 Second International Workshop on*, pp. 65 –70, April 2010.

[25] John A. Goree., "29:128 Electronics Laboratory Manual," *Department of Physics and Astronomy The University of Iowa*, pp. 84 –94, Dec 2006.

[26] Brandon David Rumberg, "Speech Processing Front-end in Low-power Hardware," M.S. thesis, West Virginia University, Morgantown,West Virginia, 2009.

[27] J. Polastre, R. Szewczyk, and D. Culler, "Telos: enabling ultra-low power wireless research," *Information Processing in Sensor Networks, 2005. IPSN 2005. Fourth International Symposium on*, pp. 364 – 369, April 2005.

[28] J. David Pfeiffer, "Find the energy contained in standard battery sizes," *http : //www.allaboutbatteries.com/index.html*. All About Batteries Website, June, 2004. Web. 30 Sep 2010.≺ http://www.allaboutbatteries.com/Energy-tables.html ≻.

[29] Wei Ye, Fabio Silva, and John Heidemann, "Ultra-low duty cycle mac with scheduled channel polling," *SenSys'06*, pp. 321–334, 2006.

[30] Joseph Polastre, Jason Hill, and David Culler, "Versatile low power media access for wireless sensor networks," *SenSys'04*, pp. 95–107, 2004.